Published OnlineFirst June 3, 2011; DOI:10.1158/1078-0432.CCR-10-3131

Translational Relevance

IGF-IR signaling is important for tumorigenicity and progression of many cancers and *k-ras* mutation is one of key factors in gastrointestinal cancers. Drugs targeting for IGF-IR pathways is in trial evaluation. In this report, we revealed that the IGF-IR monoclonal antibody, figitumumab (CP-751,871), inhibited signal transduction, proliferation, and survival of 6 gastrointestinal cancer cell lines. Moreover, in addition to its monotherapy, the combination of figitumumab and chemotherapies was highly effective against these xenograft tumors on mice. The effect of figitumumab is not influenced by the mutation status of *k-ras*. This study suggests that figitumumab may have therapeutic value in human gastrointestinal carcinomas even in the presence of *k-ras* mutations.

IGFs stimulate the proliferation of GI cancer cells and blocking of IGF-IR signaling inhibits tumor growth (9, 12–20). High serum concentration of IGF-I increases the risk of developing several cancers (10). IGF-I can also antagonize the antiproliferative effects of cyclooxygenase-2 (COX-2) inhibitors (21). Soluble IGF-IIR salvages Apc (Min/+) intestinal adenoma progression induced by loss of IGF-II imprinting (11). IGF-IR is also important for tumor maintenance in addition to carcinogenicity (22, 23). Intestinal fibroblast-derived IGF-II has been shown to stimulate proliferation of intestinal epithelial cells (24). IGF-II, in conjunction with IGF-IR, IGF-I, COX-2, and matrilysin (matrix metalloproteinase-7), seems to play a key role in the early stages of colorectal carcinogenesis (25, 26). IGF-IR signaling is also critical in tumor dissemination through the control of adhesion, migration, and metastasis. Matrilysin can cleave all 6 IGFBPs and can thus cause activate IGF signals (27, 28). We have previously reported a positive feedback loop between the IGF/IGF-IR axis and matrilysin in the invasiveness and progression of GI cancers (29).

The insulin receptor (InsR) is also another key molecule of the IGF signaling pathway and leads cell proliferation as well as affecting glucose metabolism. In addition to insulin, InsR can also bind IGF-II and initiate mitogenic signals (30). IGF-IR and InsR can form hybrid receptors that bind IGFs at physiologic concentrations. InsR and these hybrid receptors may also be involved in tumor as both insulin and IGF-I contribute to the development and progression of adenomas (31).

There are several possible approaches to blocking the IGF-IR axis. Humanized or human mAbs and TKIs for IGF-IR are available and some are in phase trials (32–34). We have constructed 2 dominant negative inhibitors for IGF-IR (IGF-IR/dn), which are active as plasmids and recombinant adenovirus vectors for several GI malignancies (15, 35–37). Figitumumab (CP-751,871) is a highly specific, fully human mAb that inhibits ligand-induced IGF-1R autophosphorylation (32). Phase 1 trials reveal that this mAb has a favorable pharmacodynamic profile and is well tolerated as a single drug without dose-limiting toxicities (38, 39). Figitumumab is also tolerable in combination with paclitaxel, carboplatin, or docetaxel (40, 41). There are only 3 reports about the efficacy of figitumumab on human GI malignancies, 1 colorectal cancer cell line, colo205, and 2 clinical studies for patients with solid tumors, including esophageal, gastric, and colon cancers and GI stromal tumor (32, 38, 42). As GI cancers are heterogeneous diseases, we decided to analyze the utility of this compound in several human GI cancer cell lines.

On the other hand, cetuximab, which is a mAb for epidermal growth factor receptor, is a useful drug for patients with colorectal cancer, however, it is not effective for tumors bearing *k-ras* mutations (43, 44). Mutation in *k-ras* is a critical genetic change, as the incidence of *k-ras* mutation is 40% to 45% in colon cancer and around 90% in pancreatic cancer. However, there is no report regarding the efficacy of IGF-IR targeting therapies for *k-ras* mutated cancers.

In this study, we assessed the impact of figitumumab on signaling blockade, growth, apoptosis-induction, and *in vivo* therapeutic efficacy in s.c. xenografts for GI cancers. We also analyzed the effects of this drug in cell lines with *k-ras* mutations. These observations strengthen the rationale for using figitumumab alone or in combination with chemotherapy in the molecular targeted therapy of GI cancers.

Materials and Methods

Materials, cell lines, and mice

Anti-Akt1(c-20), anti-ERK1(K-23), anti-phospho-ERK1 (E-4), ant-IGF-I(G-17), anti-IGF-IRα(2C8), and anti-IGF-IRβ(C20) were purchased from Santa Cruz Biotechnology and anti-phospho-Akt(Ser473), anti-phospho-p44/42-MAPK(Thy202/Tyr204), and PathScan Multiplex Western Cocktail-I were from Cell-Signaling Technology. 5-Fluorouracil (5-FU) was purchased from Sigma. Recombinant human IGF-I and IGF-II was purchased from R&D systems. All human GI cancer cell lines, colon adenocarcinomas, HT29 and DLD-1; pancreatic adenocarcinomas, BxPC3 and MIAPaca2; esophageal squamous cell carcinoma (ESCC), TE-1; and hepatoceller carcinoma, PLC/PRF/5 were obtained from Japanese Cancer Collection of Research Bioresources Cell Bank. Cells were passaged in RPMI1640 and DMEM with 10% FBS. Specific-pathogen-free female BALB/cAnNCrj-nu mice, 6-weeks-old, were purchased from Charles River. The care and use of mice were according to our university's guidelines.

A new monoclonal antibody for IGF-IR, figitumumab (CP-751,871), was kindly provided by Pfizer.

Western blotting

To analyze the duration of efficacy of this antibody, cells were cultured with media containing 0.1% bovine serum albumin and were incubated several hours with 1 μg/mL figitumumab before ligand stimulation. To assess the concentration of figitumumab required to block

Published OnlineFirst June 3, 2011; DOI:10.1158/1078-0432.CCR-10-3131

ligand-induced signal transduction, cells were cultured with media containing 0.1% bovine serum albumin and were incubated 0.5 to 3 hours with several concentrations of this mAb before stimulation.

Cells were treated with 20 ng/mL IGF-I, 40 ng/mL IGF-II, or 10 nmol/L insulin 5 minutes. Cell lysates were prepared as described previously (35). Equal aliquots of lysates (100 μg) were separated by 4% to 20% SDS-PAGE and immunoblotted onto polyvinylidene Hybond-P membrane (Amersham). Analysis was performed using indicated antibodies, and bands visualized by ECL (Amersham).

Colony-forming activity

Cells (3×10^3/plate) were seeded onto 60 mm culture plates and incubated for 24 hours. The cells were then treated with figitumumab and were incubated for 14 days. After air drying, cells were fixed with methanol and stained with Giemsa solution. Colonies containing 50 cells or more were counted.

Assessment for apoptosis

The caspase-3 colorimetric protease assay was performed following the manufacturer's protocol (MBL). In brief, the caspase-3 activity of lysates (100 μg) was measured by colorimetric reaction at 400 nm. Early apoptosis were quantified by staining with Anexin-V-FITC, according to the manufacturer's protocol (BD Biosciences) and measured by flow cytometry. TUNEL assays were performed with *in situ* apoptosis detection kit (Takara), following the manufacturer's protocol.

***In vivo* therapeutic efficacy in established tumors**

A total of 1×10^6 GI cancer cells were s.c. injected into nude mice. After tumors were palpable, animals were treated with intraperitoneal (i.p.) injection of 125 μg figitumumab, twice a week or control. Tumor diameters were serially measured with calipers and tumor volume was calculated using the formula: tumor volume (mm^3) = (width^2 × length)/2.

After GI tumors were palpable, animals were treated with i.p. injection of 125 μg figitumumab, twice a week or control. Both groups were then divided into pair-matched cytotoxic drugs, 50 mg/kg 5-FU (administered i.p. once per week) or 100 mg/kg gemcitabine (i.p., twice a week), treated and control groups. Mice were euthanized when tumors reached 2 cm in size or they developed clinically evident symptoms.

Immunohistochemical analysis

Sections (5 μm) from formalin-fixed, paraffin-embedded tumor xenografts were prepared. After removed paraffin, the sections were pretreated with Dako-Cytomation Target Retrieval Solution (Dako) in a microwave (10 minutes). Then, endogenous peroxidase activity was blocked. Antibodies were applied after blocking with normal goat serum. Sections were incubated with the anti-rabbit secondary antibody (Santa Cruz Biotechnology) and a streptavidin-HRP (Dako) followed by exposure to the diaminobenzidine tetrahydrochloride substrate (Dako).

ELISA

Serum concentrations of IGF-I, GH, insulin, and IGFBP-3 were measured using the following ELISA kits, following the manufacturer's protocols; mouse IGF-I Quantikine (R&D Systems), mouse growth hormone kit (Uscn Life Science & Technology), mouse insulin kit (Shibayagi), and mouse- and rat-IGFBP-3 ELISA (Mediagnost).

Statistical analysis

The results are presented as mean ± SE for each sample. The statistical significance of differences was determined by Student's 2-tailed *t* test in 2 groups and done by 1-way ANOVA in multiple groups, and 2-factor factorial ANOVA. *P* values of less than 0.05 were considered to indicate statistical significance.

Results

Blockade of signal transduction

To investigate the effect of figitumumab on the IGF/receptor axis, we examined 2 GI cancer cell lines, a pancreatic cancer cell, BxPC3 and a colorectal cancer cell line, HT29, which we used to evaluate the efficacy of IGF-IR blockade in the previous studies (36, 37). First, we assessed effects of figitumumab in BxPC3 on activation of IGF-IR and its downstream signals by immunoblotting. Low concentration of 0.1 μg/mL figitumumab blocked IGF-I–induced phosphorylation of both IGF-IR and Akt-1 and reduced phosphorylation of ERKs (Fig. 1A).

Similarly, in HT29 cells, figitumumab eliminated ligand-induced IGF-IR autophosphorylation and phosphorylation of both downstream, Akt-1 and ERKs (Fig. 1B). The results indicate that this mAb might effectively inhibit the IGF axis in both BxPC3 and HT29.

Then, the effect of figitumumab on a hepaloma cell line, PLC/PRF/5, was assessed (Fig. 1C). This mAb blocked both IGF-IR downstream signals of Akt-1 and ERKs with a dose dependency. One μg/mL figitumumab blocked autophosphorylation of IGF-IR and the downstream signals from 1 to 48 hours.

The *in vitro* effect on cell growth and survival

Then we analyzed the effect of this drug on *in vitro* growth and survival. One μg/mL figitumumab dramatically reduced the *in vitro* tumorigenicity of 3 cell lines as assessed by the colony formation assay (Fig. 2A).

Annexin-V assays revealed that this mAb up-regulated ethanol-induced early apoptosis synergistically in HT29 (Fig. 2B). Then we evaluated the effect of this drug on chemotherapy-induced apoptosis. Caspase-3 assay revealed that figitumumab enhanced 5-FU induced apoptosis synergistically in both HT29 and BxPC3 (Fig. 2C). The antibody strengthened additively the effect of gemcitabine

Published OnlineFirst June 3, 2011; DOI:10.1158/1078-0432.CCR-10-3131

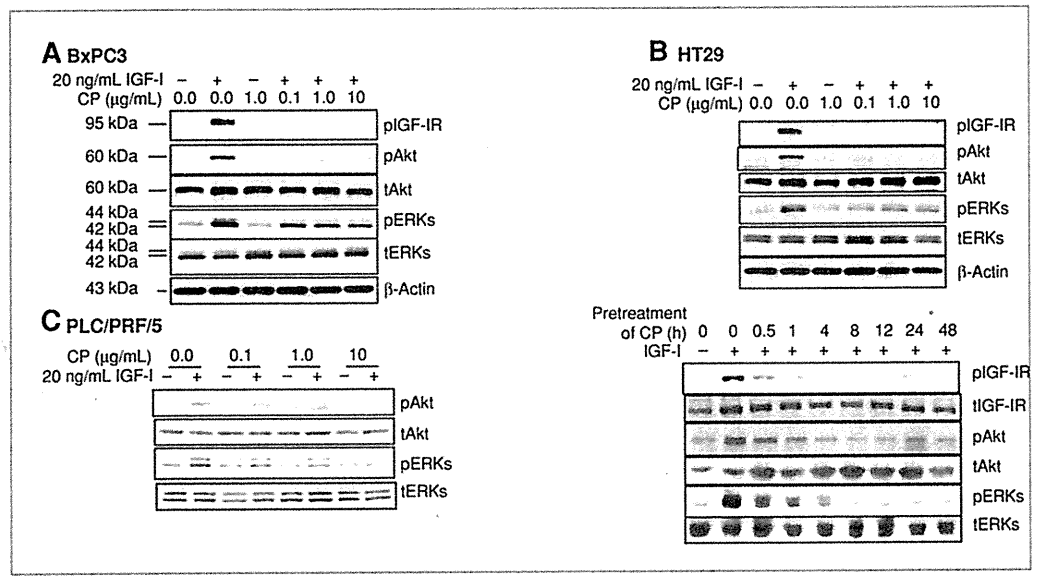

Figure 1. Two gastrointestinal cancer cell lines, pancreatic adenocarcinoma, BxPC3 (A), and colorectal adenocarcinoma, HT29 (B) were cultured with different doses of figitumumab 30 minutes, then were stimulated with 20 mg/mL IGF-I 5 minutes. Western blotting shows that CP-751,871 blocks IGF-I–induced autophosphorylation of IGF-IR completely in both cells. Figitumumab terminated IGF-I–induced activation of and Akt-1, but not ERKs completely. C, in hepatocellular carcinoma, PLC/PRF/5, ligand induced both phospholyration of Akt and ERKs were blocked by 3 hours treatment with this mAb. With incubation with 1 μg/mL figitumumab from 1 to 48 hours, this agent effectively blocked IGF-I–stimulated autophosphorylation of IGF-IR and both activation of Akt and ERKs in PLC/PRF/5.

in BxPC3 and that of 5-FU in PLC/PRF/5 (Fig. 2C). These data suggest that figitumumab might have several *in vitro* antitumor effects on GI cancer cells.

Figitumumab suppresses xenograft tumors

To analyze the effect of this drug on *in vivo* GI cancer, HT29 cells were inoculated s.c. in nude mice and allowed to

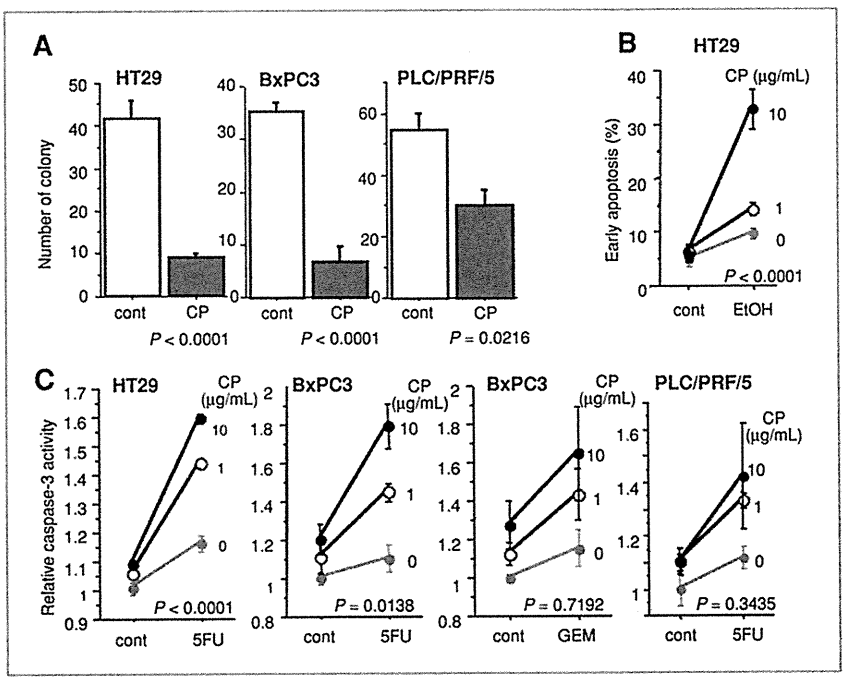

Figure 2. The effects of figitumumab on colony formation and apoptotic induction. A, colony formation assay shows that 1 μg/mL CP-751,871 reduced the number of colony of 3 GI cancer cell lines. B, Anexin-V assay reveled that CP-751,871 strengthen ethanol induced apoptosis synergistically in HT29. C, caspase-3 assay shows that CP-781871 enhanced 5-FU induced apoptosis synergistically in HT29 and BxPC3, and did additively in PLC/PRF5. Cont, control; CP, CP-751,871 (figitumumab); Gem, gemcitabine.

Published OnlineFirst June 3, 2011; DOI:10.1158/1078-0432.CCR-10-3131

form evident tumors. HT29 tumor-bearing mice were treated with i.p. injections of 125 μg figitumumab (twice a week) along with 5-FU or PBS. Although either 5-FU or figitumumab tended to suppress tumor growth, the combination therapy was much more effective than either treatment alone (Fig. 3A). Then, BxPC3 cells were inoculated in nude mice. Figitumumab monotherapy reduced the tumor growth rate of BxPC3; however, the combination with this drug and gemcitabine most effectively suppressed growth among all tested groups (Fig. 3B). However, both murine body weight and serum glucose concentration on sacrifice were not different among the 4 groups of mice.

Serum concentrations of IGF axis ligands were assessed by ELISA at the time of sacrifice. As sample number and volume were limited, we analyzed those in 2 groups, figitumumab or control ($n = 8$). Concentrations of serum IGF-I, growth hormone, insulin, and IGFBP3 were not significantly different between the 2 groups (Fig. 3C).

Resected tumor samples were investigated by immunohistochemical and TUNEL assays (Fig. 3D). The expression of IGF-IR was suppressed in BxPC3 by figitumumab monotherapy and in the both cell lines by the combination therapy. Although all treatments suppressed InsR in HT29, only the combination up-regulated InsR in BxPC3. Both 5-FU and figitumumab induced apoptosis in HT29

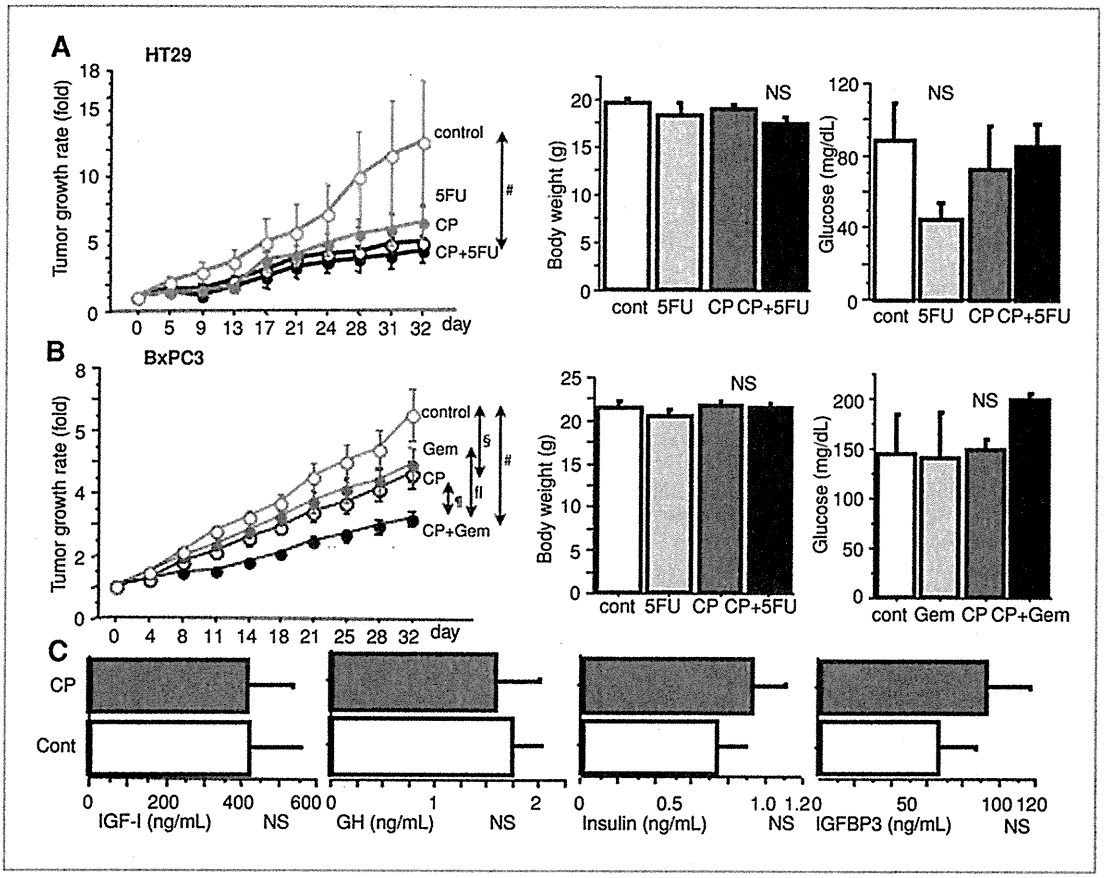

Figure 3. The effect of figitumumab on established tumor on mice. A, 125 μg CP-751,871 (twice a week, i.p.) tended to reduce relative size of s.c. tumors of HT29 on nude mice. The combination of CP-751,871 and 5-FU (once a week, i.p.) suppressed tumor growth (#, $P = 0.0268$ compared to control, each group $n = 8$). There are no significant differences between each single therapy and the combination. There are not significant differences in both body weight and blood glucose level on sacrifice (B) CP-751,871 alone reduced relative size of BxPC3 tumors on nude mice (§, $P = 0.0133$ compared to control, each group $n = 8$). The combination with CP-751,871 and gemcitabine blocked tumor growth most (#, $P < 0.0001$ compared to control). The effects of combination were more than the monotherapies (¶, $P = 0.0274$ compared to mAb; fl, $P = 0.0036$ to gemcitabine). Both body weight and blood glucose level on sacrifice were not different among 4 groups. C, ELISA showed that CP-751,871 did not affect blood concentrations of IGF-I (mean ± SE in mice treated with CP-751,871 was 415 ng/mL ± 122 and that in mice treated with control was 420 ng/mL ± 137, $P = 0.9775$), growth hormone (1.58 ng/mL ± 0.42 and 1.74 ng/mL ± 0.27, respectively, $P = 0.7470$), insulin (0.92 ng/mL ± 0.19 and 0.73 ng/mL ± 0.16, respectively, $P = 0.4446$), and IGF binding protein-3 (92. 07 ng/mL ± 24.92 and 66.45 ng/mL ± 20.97, respectively, $P = 0.4446$) on sacrifice.

Published OnlineFirst June 3, 2011; DOI:10.1158/1078-0432.CCR-10-3131

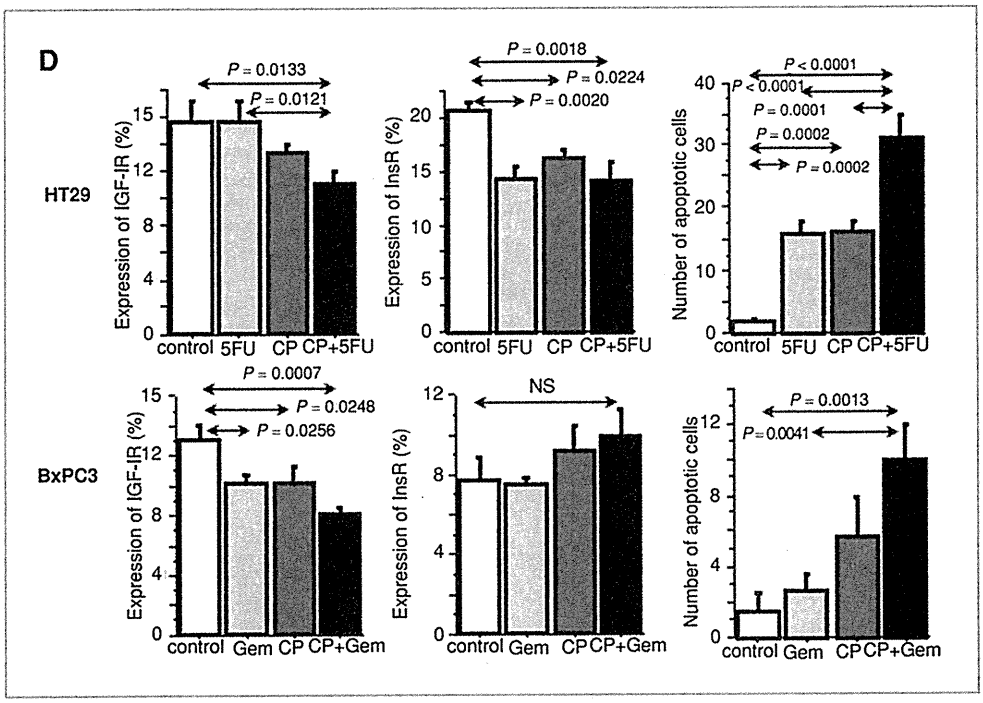

Figure 3. (*Continued*) D, receptors expressions and apoptosis induction in SC tumors on sacrifice were assessed by immunostaining. CP-751,871 alone reduced the expression of IGF-IR in BxPC3 tumors but not in HT29. Combination treatments reduce both expression of IGF-IR in both cell types and InsR in HT29, but up-regulated InsR in BxPC3. TUNEL assay shows that CP-751, 871 induced apoptosis in HT29 and enhanced both gemcitabine and 5-FU induced apoptosis. *Post hoc t* test was by Fischer's PLSD. Cont, control; CP, CP-751,871 (figitumumab); Gem, gemcitabine.

xenografts, and the number of apoptotic cells was greatest in the combination group. In BxPC3 xenografts, figitumumab up-regulated gemcitabine-induced apoptosis, although each individual treatment did not induce apoptosis significantly.

The results indicate that figitumumab might be effective for GI cancers, HT29 and BxPC3; however, both cell lines have wild-type *k-ras* so we asked whether the same effects could be observed in *k-ras* mutant cell lines.

Blockade of signal transduction in *k-ras* mutated cells

It has been reported that *k-ras* mutation is one of key genetic events in GI malignancies, and is associated with significant resistance to molecular targeted therapies such as cetuximab (44). There is therefore a dearth of novel and effective therapies in this subset of tumors. To assess the effect of figitumumab on the IGF/receptor axis in GI cancers with *k-ras* mutation, we examined 3 GI cancer cell lines, DLD-1, MIAPaca2, and TE-1 with this mutation. One μg/mL figitumumab blocked autophosphorylation of IGF-IR from 1 to 48 hours in all 3 cell lines (Fig. 4A). Downstream signals of Akt-1 and the ERKs were also blocked by 1 μg/mL figitumumab. Although the effect of this mAb on the ERKs showed dose dependency in all 3 cell lines, a low dose of 0.1 μg/mL figitumumab blocked Akt effectively (Fig. 4B). These data show that figitumumab can block IGF-I signals in GI cancers with *k-ras* mutations.

In addition to IGF-I, 1 μg/mL figitumumab blocked IGF-II induced both phosphorylation of Akt and ERKs in DLD-1 (Fig. 4C). The results indicate that this mAb can block IGF signals effectively for GI malignancies having a mutation in *k-ras*.

The effect of this antibody on insulin signaling was limited. High doses of 10 μg/mL figitumumab could block insulin-induced autophosphorylation of InsR and activation of Akt-1, but not that of ERKs in DLD1 (Fig. 4D). One μg/mL figitumumab did not inhibit insulin signals between 30 minutes and 48 hours exposures in DLD1.

The *in vitro* effect on cell growth and survival for *k-ras* mutated cells

Next, we assessed the effect of this drug on the *in vitro* growth and survival of *k-ras* mutated GI cancers. Colony formation assays showed that this mAb reduced the *in vitro* tumorigenicity of both DLD1 and MIAPaca2 in a dose-dependent fashion (Fig. 5A). One μg/mL figitumumab also effectively reduced colony formation of TE1.

Caspase-3 assays revealed that this antibody enhanced 5-FU induced apoptosis synergistically in DLD1 and additively in the other cell lines, MIAPaca2 and TE1 (Fig. 5B).

Published OnlineFirst June 3, 2011; DOI:10.1158/1078-0432.CCR-10-3131

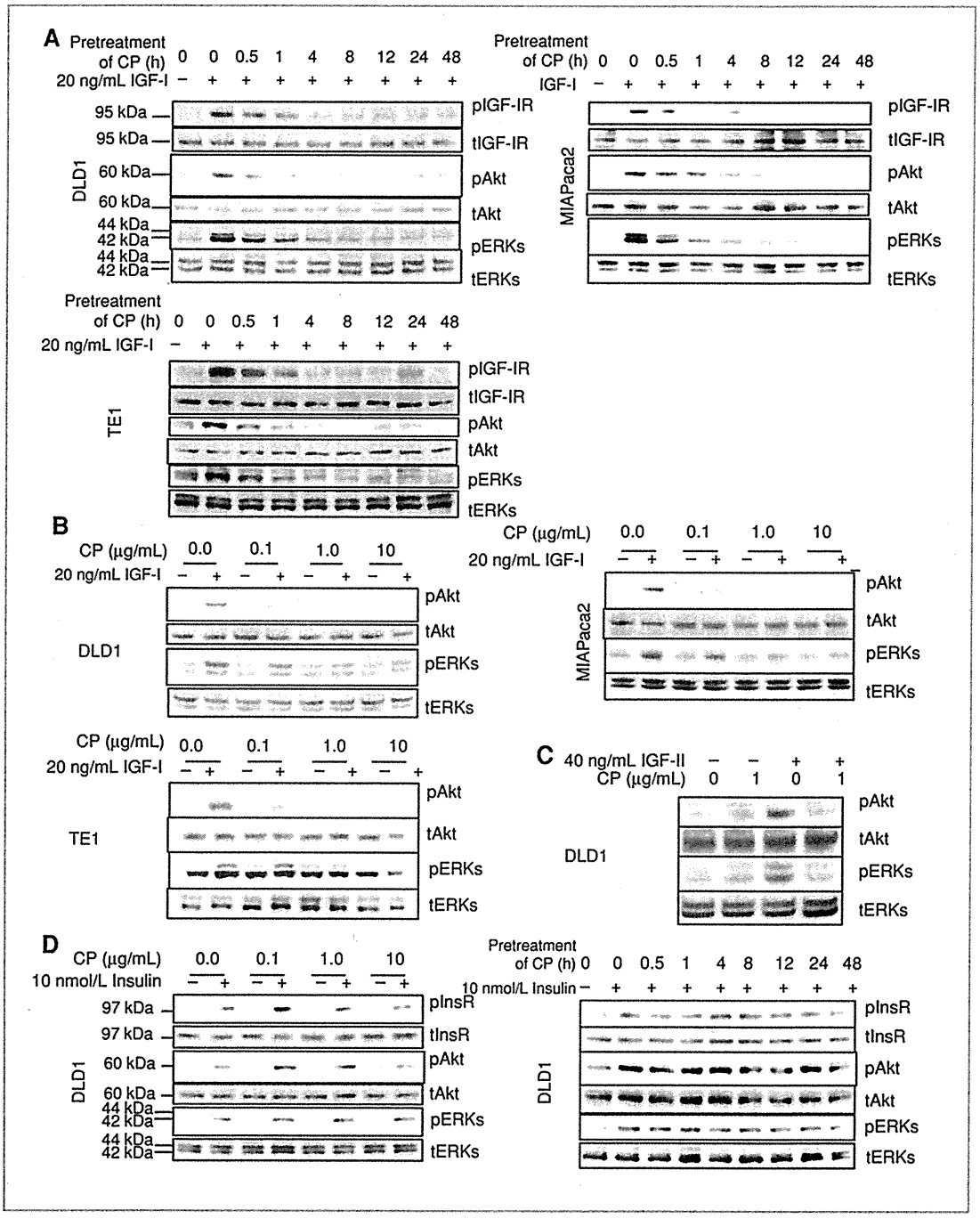

Figure 4. The effect of signal transduction on gastrointestinal cancer cells with *k-ras* mutation. A, with incubation with 1 μg/mL figitumumab from 1 to 48 hours, this mAb effectively blocked IGF-I–stimulated autophosphorylation of IGF-IR and both activation of Akt and ERKs in 3 cell lines; colorectal adenocarcinoma, DLD-1; pancreatic adenocarcinoma, MIAPaca2; and esophageal squamous cell carcinoma, TE1. B, ligand induced phospholyration of down-stream, Akt and ERKs, was blocked by 3 hours treatment with figitumumab, the former tend to be seen in lower dose of figitumumab than the latter. C, in DLD-1, this mAb blocked IGF-II stimulated both phosphorylation of Akt and ERKs. D, to block 10 nmol/L insulin-induced signal transduction, more than 10 μg/mL figitumumab (3 hours incubation) are needed in DLD-1.

Published OnlineFirst June 3, 2011; DOI:10.1158/1078-0432.CCR-10-3131

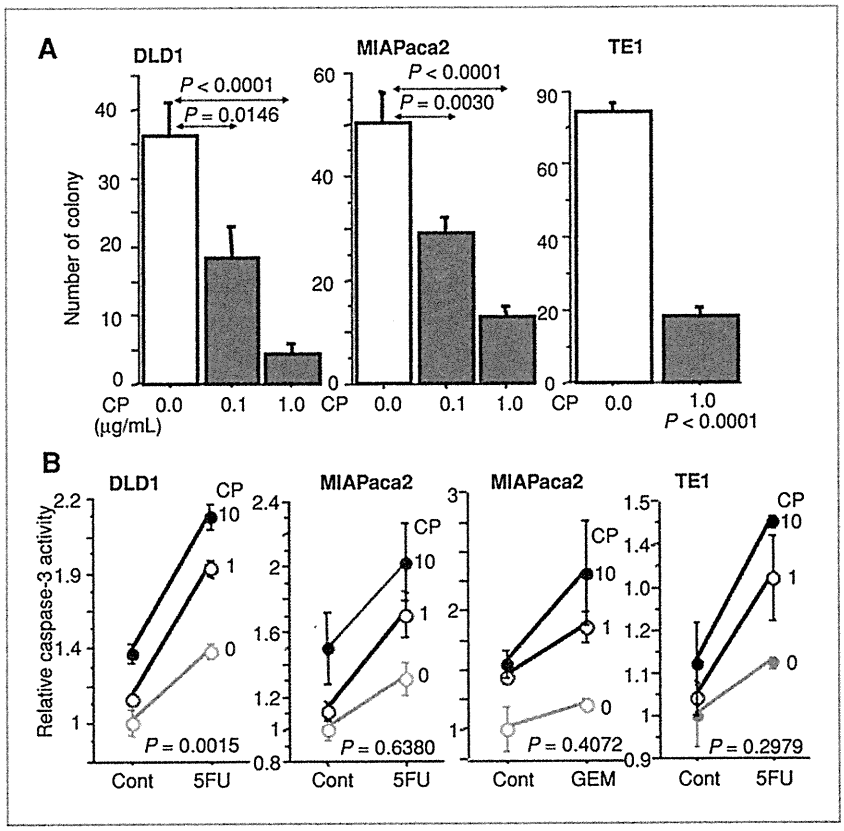

Figure 5. The effect of figitumumab on colony formation and survival in *k-ras* mutated GI cancer cells. A, the mAb reduced colony formation with dose dependency in both DLD-1 and MIAPaca2. One μg/mL figitumumab effectively blocked colony formation in TE1. B, caspase-3 assay shows that CP-781871 enhanced chemotherapy induced apoptosis; synergistically with 5-FU in DLD-1, and additively with gemcitabine in MIAPaca2 and with 5-FU in MIAPaca2 and TE1.

This drug strengthened the effect of gemcitabine additively in MIAPaca2. These results suggest that figitumumab has significant antitumor effects on GI cancer cells with *k-ras* mutations.

Figitumumab suppressed *k-ras* mutated tumors in mice

To assess the *in vivo* effect of this drug on GI cancers with *k-ras* mutations, DLD1 cells were inoculated s.c. in nude mice and allowed to form evident tumors. DLD1 tumor-bearing mice were treated with an i.p. injection of 125 μg figitumumab (twice a week) or control. This mAb suppressed tumor growth significantly (Fig. 6A). Then, the combination effect of this antibody and 5-FU was assessed. This combination suppressed tumor growth more effectively than monotherapy, however these additive effects were limited. None of these treatments affected murine body weight on sacrifice.

The *in vivo* effect of figitumumab on another *k-ras* mutated cell line, MIAPaca2, was then assessed. This drug inhibited dramatically tumor growth of MIAPaca2 xenografts (Fig. 6B). Both monotherapies of figitumumab and gemcitabine clearly reduced tumor growth ($P = 0.0036$ and 0.0012 compared to control, respectively), however the combination inhibited growth more effectively ($P <$ 0.0001). Although treatment with gemcitabine was associated with reduced murine weight on sacrifice, the mAb alone did not affect animal weight. Figitumumab increased serum glucose concentrations on sacrifice more than gemcitabine monotherapy.

To assess the effect of treatments on both cell proliferation and apoptosis, resected tumor tissues were analyzed (Fig. 6C). In DLD1 tumors, only the combination therapy effectively reduced cell proliferation. In MIAPaca2 tumors, gemcitabine down-regulated proliferation, which was enhanced by figitumumab. In DLD1 tumors, 5-FU induced apoptosis and this antibody increased this effect. In MIAPaca2 tumors, gemcitabine induced apoptosis and this mAb up-regulated this effect. These results suggest that the antitumor effects of figitumumab are observed even in the presence of *k-ras* mutation in GI cancers.

Discussion

GI carcinomas are composed of a variety of histological types, and patients with these cancers show vastly different clinical courses. GI cancers are often diagnosed in advanced stages having lymph node/distant metastases and peritoneal dissemination, and in these cases there are extremely limited

Published OnlineFirst June 3, 2011; DOI:10.1158/1078-0432.CCR-10-3131

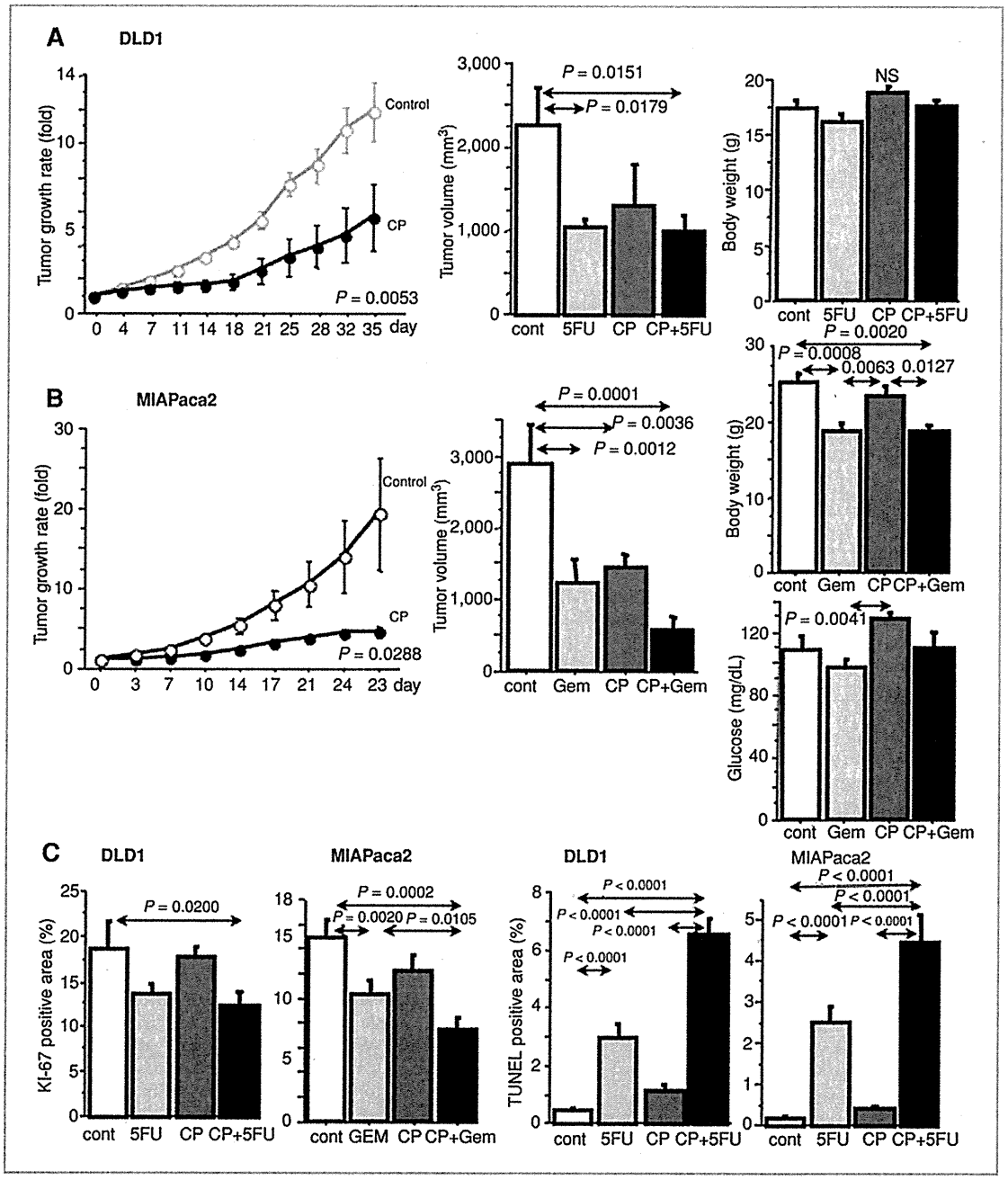

Figure 6. The effects of figitumumab on *k-ras* mutated GI cancer on mice. A, figitumumab suppressed tumor growth rate of DLD-1 on mice ($n = 8$, $P = 0.0053$). Tumor volume of mice treated with combination of this mAb and 5-FU showed least of all groups ($P = 0.0151$, the combination vs. control, each group $n = 8$), however there are no significant differences between each monotherapy and the combination. Body weight of mice on sacrifice was not influenced by treatments. B, figitumumab inhibited tumor growth rate of MIAPaca2 on mice ($n = 8$, $P = 0.0288$). The combination of this antibody and gemcitabine suppressed tumor volume most effectively of all ($P < 0.0001$, the combination vs. control, each group $n = 8$), however there are no significant differences between each monotherapy and the combination. Gemcitabine decreased murine weight on sacrifice and figitumumab single therapy up-regulated blood glucose on sacrifice. C, the combination treatment reduced Ki-67 label in DLD1. Gemcitabine alone reduce tumor cell growth and figitumumab enhanced this effect. In both tumors, 5-FU induced TUNEL positive area and figitumumab strengthened this effect. *Post hoc t* test was by Fischer's PLSD. Cont, control; CP, CP-751,871 (figitumumab); Gem, gemcitabine.

Published OnlineFirst June 3, 2011; DOI:10.1158/1078-0432.CCR-10-3131

options. GI malignancies are thus higher in overall mortality rates compared to their incidence rates (1). IGF-mediated growth-responsiveness is found in most GI cancer cells, including esophagus, intestine, pancreas, and liver (12, 15, 16, 19). High expression of both IGF-IR and the ligands in tumor tissues has indicated continuous activation of this system by paracrine and autocrine loops (19, 45). The expression of IGF-IR/IGF-II might be useful for the predictive marker of recurrence and poor prognosis in ESCC (15). The functional significance of IGF-IR has been showed as cancer growth inhibition by anti–IGF-IR antibodies (19, 32). Here, we used a new IGF-IR mAb, figitumumab, for the accurate dissection of the responsible signaling pathways. The results indicate that this strategy is promising for the treatment of GI tumors, not only as a monotherapy but especially in combination with cytotoxic drugs. We first showed that figitumumab enhanced the effects of both 5-FU and gemcitabine. Resistance to chemotherapy is a serious problem in patients with GI malignancies and this approach has the potential for overcoming this difficulty. It is important to note that our studies show that figitumumab is effective against a wide range of GI carcinomas, and these effects are not unique to 1 or 2 unusual cell lines.

Cetuximab is a powerful molecular targeted drug for patients with colorectal cancer, however, it shows limited or no efficacy for *k-ras* mutated cancers(43, 44). Although IGF-IR might be the next important target in human GI carcinomas, there is no information about IGF-IR–targeted therapy in *k-ras* mutated cancers. In this study, figitumumab showed antitumor effects for *k-ras* mutated cancers as well as wild-type ones both *in vitro* and *in vivo*. Our previous data in GI carcinomas indicated that IGF-IR blockade inhibited Akt signals more than ERK signaling, so the PI3-K/Akt pathway might play a more important role than the ras/MAPK pathway in the downstream signals of the IGF/IGF-IR axis (15, 35–37). This could explain why figitumumab is active for *k-ras* mutated GI cancer cells, however further studies are needed to analyze this mechanism precisely. Although we did not assess the efficacy of this drug for patients with GI cancers with and without *k-ras* mutations, these data might support the use of this mAb in this clinical setting. Further studies will be needed to clarify this hypothesis.

A major obstacle to the targeting of IGF-IR is the close homology of the IGF-IR and the IR kinase domains (46). Therefore, it is important that any strategy designed to block IGF signaling has specificity for IGF-IR and without a detrimental influence on IR signals. We show here that figitumumab does not suppress insulin-induced InsR- or Akt-phosphorylation in DLD1 indicating a high degree of receptor selectivity at tumor-active doses with this molecular-targeted therapy. Plasma concentrations of glucose, IGF-I, insulin, growth hormone, IGFBP3 were not influenced by this mAb. Moreover, body weight was monitored and not significantly affected by this therapy. This lack of effect on the insulin pathway and clinical toxicity leads us to believe that these combinations will have minimal adverse effects in clinical applications.

As figitumumab is of the IgG2 subtype, which is usually a poor activator of cellular immune responses, ongoing clinical trials may clarify whether this agent has significantly different properties from the IgG1 class from which class most other mAbs targeting IGF-IR are derived. According to several clinical studies, the main adverse effects of IGF-IR mAb are hyperglycemia, mild skin toxicities, and fatigue (41, 47, 48). IGF-IR mAb has been reported to cause hyperglycemia in about 20% of patients but this has generally been tolerable, mild to moderate, reversible, and manageable with usual oral hypoglycemic drugs. Patients with previous glucose intolerance or with steroids usage might be at increased risk of hyperglycemia.

It is also important to define surrogate markers of response for modern targeted agents. Although we could not assess this completely in these murine models, several possibilities have been put forward. One is that circulating tumor cells would be a marker, as treatment with figitumumab decreased both total circulating tumor cell count and IGF-IR–positive circulating tumor cell count (41). Another is that high concentration of serum-free IGF-I may be a marker of high responder of patients with non small cell lung carcinoma treated with figitumumab.

Recently, a new role of the IGF-IR has been identified that there is significant cross-talk between the IGF-IR and other tyrosine kinase receptors. For example, many patients with breast cancer who achieve an initial response to trastuzumab acquire secondary resistance. One mechanism of resistance has been showed to be overexpression of IGF-IR (49) and another is the formation of IGF-IR/Her2 heterodimers (50). These data suggest that IGF-IR blockade may be specifically effective for breast cancer patients with trastuzumab-resistant tumors.

Thus, in this study, we show that figitumumab suppresses the tumorigenicity and survival of GI cancers with or without *k-ras* mutations, by blocking Akt and ERK activation, both *in vitro* and in animal models. It also enhances chemotherapy efficacy without significantly influencing InsR signals at therapeutically effective doses. This study thus validates IGF-IR as a therapeutic target in GI carcinomas and suggest that figitumumab may be a promising antitumor therapeutic for these diseases.

Disclosure of Potential Conflicts of Interest

No potential conflicts of interest were disclosed.

Grant Support

This work was supported by grants-in-aid from the Ministry of Education, Culture, Sports, Science, and Technology and from the Ministry of Health, Labour and Welfare, Japan.

The costs of publication of this article were defrayed in part by the payment of page charges. This article must therefore be hereby marked *advertisement* in accordance with 18 U.S.C. Section 1734 solely to indicate this fact.

Received November 23, 2010; revised May 19, 2011; accepted May 24, 2011; published OnlineFirst June 3, 2011.

Published OnlineFirst June 3, 2011; DOI:10.1158/1078-0432.CCR-10-3131

References

1. American Cancer Society. Cancer Facts & Figures 2010. Available from: http://wwwcancerorg/acs/groups/content/@epidemiologysurveilance/documents/document/acspc-026238pdf2010.
2. Baserga R. Oncogenes and the strategy of growth factors. Cell 1994;79:927–30.
3. Adachi Y, Yamamoto H, Imsumran A, et al. Insulin-like growth factor-I receptor as a candidate for a novel molecular target in the gastrointestinal cancers. Dig Endosc 2006;18:245–51.
4. Miller BS, Yee D. Type I insulin-like growth factor receptor as a therapeutic target in cancer. Cancer Res 2005;65:10123–7.
5. Ullrich A, Gray A, Tam AW, Yang-Feng T, Tsubokawa M, Collins C, et al. Insulin-like growth factor I receptor primary structure: comparison with insulin receptor suggests structural determinants that define functional specificity. Embo J 1986;5:2503–12.
6. Baselga J, Norton L, Albanell J, Kim YM, Mendelsohn J. Recombinant humanized anti-HER2 antibody (Herceptin) enhances the antitumor activity of paclitaxel and doxorubicin against HER2/neu overexpressing human breast cancer xenografts. Cancer Res 1998;58:2825–31.
7. Yu H, Rohan T. Role of the insulin-like growth factor family in cancer development and progression. J Natl Cancer Inst 2000;92:1472–89.
8. Sara VR, Hall K. Insulin-like growth factors and their binding proteins. Physiol Rev 1990;70:591–614.
9. Remacle-Bonnet M, Garrouste F, el Atiq F, Roccabianca M, Marvaldi J, Pommier G. des-(1–3)-IGF-I, an insulin-like growth factor analog used to mimic a potential IGF-II autocrine loop, promotes the differentiation of human colon-carcinoma cells. Int J Cancer 1992;52:910–7.
10. Ma J, Pollak MN, Giovannucci E, Chan JM, Tao Y, Hennekens CH, et al. Prospective study of colorectal cancer risk in men and plasma levels of insulin-like growth factor (IGF)-I and IGF-binding protein-3. J Natl Cancer Inst 1999;91:620–5.
11. Harper J, Burns JL, Foulstone EJ, Pignatelli M, Zaina S, Hassan AB. Soluble IGF2 receptor rescues Apc(Min/+) intestinal adenoma progression induced by Igf2 loss of imprinting. Cancer Res 2006;66:1940–8.
12. Lahm H, Suardet L, Laurent PL, Fischer JR, Ceyhan A, Givel JC, et al. Growth regulation and co-stimulation of human colorectal cancer cell lines by insulin-like growth factor I, II and transforming growth factor alpha. Br J Cancer 1992;65:341–6.
13. Thompson MA, Cox AJ, Whitehead RH, Jonas HA. Autocrine regulation of human tumor cell proliferation by insulin-like growth factor II: an in-vitro model. Endocrinology 1990;126:3033–42.
14. Chen SC, Chou CK, Wong FH, Chang CM, Hu CP. Overexpression of epidermal growth factor and insulin-like growth factor-I receptors and autocrine stimulation in human esophageal carcinoma cells. Cancer Res 1991;51:1898–903.
15. Imsumran A, Adachi Y, Yamamoto H, Li R, Wang Y, Min Y, et al. Insulin-like growth factor-I receptor as a marker for prognosis and a therapeutic target in human esophageal squamous cell carcinoma. Carcinogenesis 2007;28:947–56.
16. Caro JF, Poulos J, Ittoop O, Pories WJ, Flickinger EG, Sinha MK. Insulin-like growth factor I binding in hepatocytes from human liver, human hepatoma, and normal, regenerating, and fetal rat liver. J Clin Invest 1988;81:976–81.
17. Verspohl EJ, Maddux BA, Goldfine ID. Insulin and insulin-like growth factor I regulate the same biological functions in HEP-G2 cells via their own specific receptors. J Clin Endocrinol Metab 1988;67:169–74.
18. Kim SO, Park JG, Lee YI. Increased expression of the insulin-like growth factor I (IGF-I) receptor gene in hepatocellular carcinoma cell lines: implications of IGF-I receptor gene activation by hepatitis B virus X gene product. Cancer Res 1996;56:3831–6.
19. Bergmann U, Funatomi H, Yokoyama M, Beger HG, Korc M. Insulin-like growth factor I overexpression in human pancreatic cancer: evidence for autocrine and paracrine roles. Cancer Res 1995;55:2007–11.
20. Ajisaka H, Fushida S, Yonemura Y, Miwa K. Expression of insulin-like growth factor-2, c-MET, matrix metalloproteinase-7 and MUC-1 in primary lesions and lymph node metastatic lesions of gastric cancer. Hepatogastroenterology 2001;48:1788–92.
21. Levitt RJ, Pollak M. Insulin-like growth factor-I antagonizes the antiproliferative effects of cyclooxygenase-2 inhibitors on BxPC-3 pancreatic cancer cells. Cancer Res 2002;62:7372–6.
22. Baserga R. The insulin-like growth factor I receptor: a key to tumor growth? Cancer Res 1995;55:249–52.
23. Sell C, Rubini M, Rubin R, Liu JP, Efstratiadis A, Baserga R. Simian virus 40 large tumor antigen is unable to transform mouse embryonic fibroblasts lacking type 1 insulin-like growth factor receptor. Proc Natl Acad Sci U S A 1993;90:11217–21.
24. Simmons JG, Pucilowska JB, Lund PK. Autocrine and paracrine actions of intestinal fibroblast-derived insulin-like growth factors. Am J Physiol 1999;276:G817–27.
25. Nosho K, Yamamoto H, Taniguchi H, Adachi Y, Yoshida Y, Arimura Y, et al. Interplay of insulin-like growth factor-II, insulin-like growth factor-I, insulin-like growth factor-I receptor, COX-2, and matrix metalloproteinase-7, play key roles in the early stage of colorectal carcinogenesis. Clin Cancer Res 2004;10:7950–7.
26. Nosho K, Yamamoto H, Adachi Y, Endo T, Hinoda Y, Imai K. Gene expression profiling of colorectal adenomas and early invasive carcinomas by cDNA array analysis. Br J Cancer 2005;92:1193–200.
27. Nakamura M, Miyamoto S, Maeda H, Ishii G, Hasebe T, Chiba T, et al. Matrix metalloproteinase-7 degrades all insulin-like growth factor binding proteins and facilitates insulin-like growth factor bioavailability. Biochem Biophys Res Commun 2005;333:1011–6.
28. Miyamoto S, Nakamura M, Yano K, Ishii G, Hasebe T, Endoh Y, et al. Matrix metalloproteinase-7 triggers the matricrine action of insulin-like growth factor-II via proteinase activity on insulin-like growth factor binding protein 2 in the extracellular matrix. Cancer Sci 2007;98:685–91.
29. Adachi Y, Li R, Yamamoto H, Min Y, Piao W, Wang Y, et al. Insulin-like growth factor-I receptor blockade reduces the invasiveness of gastrointestinal cancers via blocking production of matrilysin. Carcinogenesis 2009;30:1305–13.
30. Pandini G, Frasca F, Mineo R, Sciacca L, Vigneri R, Belfiore A. Insulin/insulin-like growth factor I hybrid receptors have different biological characteristics depending on the insulin receptor isoform involved. J Biol Chem 2002;277:39684–95.
31. Schoen RE, Weissfeld JL, Kuller LH, Thaete FL, Evans RW, Hayes RB, et al. Insulin-like growth factor-I and insulin are associated with the presence and advancement of adenomatous polyps. Gastroenterology 2005;129:464–75.
32. Cohen BD, Baker DA, Soderstrom C, Tkalcevic G, Rossi AM, Miller PE, et al. Combination therapy enhances the inhibition of tumor growth with the fully human anti-type 1 insulin-like growth factor receptor monoclonal antibody CP-751,871. Clin Cancer Res 2005;11:2063–73.
33. Wang Y, Hailey J, Williams D, Wang Y, Lipari P, Malkowski M, et al. Inhibition of insulin-like growth factor-I receptor (IGF-IR) signaling and tumor cell growth by a fully human neutralizing anti-IGF-IR antibody. Mol Cancer Ther 2005;4:1214–21.
34. Wittman M, Carboni J, Attar R, Balasubramanian B, Balimane P, Brassil P, et al. Discovery of a (1H-benzoimidazol-2-yl)-1H-pyridin-2-one (BMS-536924) inhibitor of insulin-like growth factor I receptor kinase with *in vivo* antitumor activity. J Med Chem 2005;48:5639–43.
35. Adachi Y, Lee CT, Coffee K, Yamagata N, Ohm JE, Park KH, et al. Effects of genetic blockade of the insulin-like growth factor receptor in human colon cancer cell lines. Gastroenterology 2002;123:1191–204.
36. Min Y, Adachi Y, Yamamoto H, Ito H, Itoh F, Lee CT, et al. Genetic blockade of the insulin-like growth factor-i receptor: a promising strategy for human pancreatic cancer. Cancer Res 2003;63:6432–41.
37. Min Y, Adachi Y, Yamamoto H, Imsumran A, Arimura Y, Endo T, et al. Insulin-like growth factor I receptor blockade enhances chemotherapy and radiation responses and inhibits tumour growth in human gastric cancer xenografts. Gut 2005;54:591–600.
38. Haluska P, Shaw HM, Batzel GN, Yin D, Molina JR, Molife LR, et al. Phase I dose escalation study of the anti insulin-like growth factor-I receptor monoclonal antibody CP-751,871 in patients with refractory solid tumors. Clin Cancer Res 2007;13:5834–40.
39. Lacy MQ, Alsina M, Fonseca R, Paccagnella ML, Melvin CL, Yin D, et al. Phase I, pharmacokinetic and pharmacodynamic study of the

Published OnlineFirst June 3, 2011; DOI:10.1158/1078-0432.CCR-10-3131

anti-insulin-like growth factor type 1 Receptor monoclonal antibody CP-751,871 in patients with multiple myeloma. J Clin Oncol 2008;26:3196–203.
40. Karp DD, Paz-Ares LG, Novello S, Haluska P, Garland L, Cardenal F, et al. Phase II study of the anti-insulin-like growth factor type 1 receptor antibody CP-751,871 in combination with paclitaxel and carboplatin in previously untreated, locally advanced, or metastatic non-small-cell lung cancer. J Clin Oncol 2009;27:2516–22.
41. de Bono JS, Attard G, Adjei A, Pollak MN, Fong PC, Haluska P, et al. Potential applications for circulating tumor cells expressing the insulin-like growth factor-I receptor. Clin Cancer Res 2007;13:3611–6.
42. Molife LR, Fong PC, Paccagnella L, Reid AH, Shaw HM, Vidal L, et al. The insulin-like growth factor-I receptor inhibitor figitumumab (CP-751,871) in combination with docetaxel in patients with advanced solid tumours: results of a phase Ib dose-escalation, open-label study. Br J Cancer 2010;103:332–9.
43. Karapetis CS, Khambata-Ford S, Jonker DJ, O'Callaghan CJ, Tu D, Tebbutt NC, et al. K-ras mutations and benefit from cetuximab in advanced colorectal cancer. N Engl J Med 2008;359:1757–65.
44. Jimeno A, Messersmith WA, Hirsch FR, Franklin WA, Eckhardt SG. KRAS mutations and sensitivity to epidermal growth factor receptor inhibitors in colorectal cancer: practical application of patient selection. J Clin Oncol 2009;27:1130–6.
45. Lahm H, Amstad P, Wyniger J, Yilmaz A, Fischer JR, Schreyer M, et al. Blockade of the insulin-like growth-factor-I receptor inhibits growth of human colorectal cancer cells: evidence of a functional IGF-II-mediated autocrine loop. Int J Cancer 1994;58:452–9.
46. Adams TE, Epa VC, Garrett TP, Ward CW. Structure and function of the type 1 insulin-like growth factor receptor. Cell Mol Life Sci 2000;57:1050–93.
47. Tolcher AW, Sarantopoulos J, Patnaik A, Papadopoulos K, Lin CC, Rodon J, et al. Phase I, pharmacokinetic, and pharmacodynamic study of AMG 479, a fully human monoclonal antibody to insulin-like growth factor receptor 1. J Clin Oncol 2009;27:? 5800–7.
48. Kurzrock R, Patnaik A, Aisner J, Warren T, Leong S, Benjamin R, et al. A phase I study of weekly R1507, a human monoclonal antibody insulin-like growth factor-I receptor antagonist, in patients with advanced solid tumors. Clin Cancer Res. 2010;16:2458–65.
49. Lu Y, Zi X, Zhao Y, Mascarenhas D, Pollak M. Insulin-like growth factor-I receptor signaling and resistance to trastuzumab (Herceptin). J Natl Cancer Inst 2001;93:1852–7.
50. Nahta R, Yuan LX, Zhang B, Kobayashi R, Esteva FJ. Insulin-like growth factor-I receptor/human epidermal growth factor receptor 2 heterodimerization contributes to trastuzumab resistance of breast cancer cells. Cancer Res 2005;65:11118–28.

J Gastroenterol (2011) 46:143–152
DOI 10.1007/s00535-010-0320-7

ORIGINAL ARTICLE—ALIMENTARY TRACT

Myogenic lineage differentiated mesenchymal stem cells enhance recovery from dextran sulfate sodium-induced colitis in the rat

Hiroki Tanaka · Yoshiaki Arimura · Takashi Yabana · Akira Goto · Masayo Hosokawa · Kanna Nagaishi · Kentaro Yamashita · Hiroyuki Yamamoto · Yasushi Sasaki · Mineko Fujimiya · Kohzoh Imai · Yasuhisa Shinomura

Received: 7 June 2010 / Accepted: 13 August 2010 / Published online: 17 September 2010

Abstract
Background Although mounting evidence implicates mesenchymal stem cells (MSCs) in intestinal tissue repair, uncertainty remains concerning the distribution, function, and fate of repopulating MSCs in recipient colonic tissues. Therefore, we investigated the role of transplanted MSCs in the repair phase of DSS colitis.
Methods LacZ-labeled rat MSCs were transplanted into rats with colitis induced by 4% DSS on day 2. Regular water replaced the DSS solution on day 6. Therapeutic effect was evaluated on day 9 by clinicopathologic and growth factor/cytokine expression profiles. We analyzed the Notch signaling pathway by Western blotting and characterized immunofluorescence of lacZ-labeled MSCs with confocal laser microscopy. In vivo differentiation of MSC was confirmed by transmission electron microscopy (TEM).
Results Recovery of colitis was modestly but significantly promoted by MSC transplantation due to proceeding cell cycle and inhibiting apoptosis in the epithelia. *Tgfa* mRNA expression increased significantly, while Notch signaling was inhibited in the colonic tissues with MSC transplantation. β-Galactosidase-positive cells, which expressed α-SMA, desmin, and vimentin, were infrequently detected in the lamina propria stroma. DSS exposure in vitro proved to be the most potent inducer for α-SMA in MSCs where TEM demonstrated myogenic lineage differentiation.
Conclusions We found that MSCs transplantation modestly promoted the repair of DSS colitis. The donor-derived MSCs were likely reprogrammed to differentiate to myogenic lineage cells by cues from the micro milieu. Further characterization of these cells is warranted as a basis for applying cell-based therapy for inflammatory bowel disease.

Keywords Mesenchymal stem cell (MSC) · Myogenic lineage differentiation, dextran sulfate sodium (DSS) colitis · Recovery phase · Inflammatory bowel disease (IBD)

Electronic supplementary material The online version of this article (doi:10.1007/s00535-010-0320-7) contains supplementary material, which is available to authorized users.

H. Tanaka · Y. Arimura (✉) · T. Yabana · A. Goto · M. Hosokawa · K. Yamashita · H. Yamamoto · Y. Shinomura
First Department of Internal Medicine, Sapporo Medical University, S-1, W-16, Chuo-ku, Sapporo 060-8543, Japan
e-mail: arimura@sapmed.ac.jp

K. Nagaishi · M. Fujimiya
Department of Anatomy, Sapporo Medical University, Sapporo, Japan

Y. Sasaki
Department of Molecular Biology, Sapporo Medical University, Sapporo, Japan

K. Imai
Sapporo Medical University, Sapporo, Japan

Introduction

Dextran sulfate sodium (DSS), a heparin-like long-chain polysaccharide polymer containing up to three sulfate groups per glucose molecule, induces colitis in mice and rats when dissolved in their drinking water [1]. DSS is believed to be directly toxic to gut epithelial cells due to its marked electro-negativity and osmotic effects [2]. It

impairs epithelial barrier integrity with a subsequent Th1 skewed immune-mediated inflammation involving macrophage activation and possibly the intestinal microflora [3]. Oral DSS induces acute colitis followed by relatively slow mucosal repair, namely, a recovery phase follows cessation of DSS intake in which colonic epithelial cell hyperplasia and crypt elongation follow a dramatic increase in epithelial cell proliferation [4]. Since intestinal wound healing generally proceeds in three distinct phases [5]—epithelial cell migration called epithelial restitution [6], proliferation [7], and differentiation [8]—this feature makes the DSS model useful for studying mechanisms of colonic wound healing and the effects of therapeutic interventions. Understanding the recovery phase of DSS colitis may eventually lead to new therapies that could accelerate and promote mucosal repair in patients with active inflammatory bowel disease (IBD) [9].

Many recent reports describe the plasticity of bone marrow-derived cells (BMDCs) to repopulate and transform to various intestinal cell types [10, 11], including intestinal epithelial cells (IECs), especially of secretory lineage [12], interstitial cells [10], including subepithelial myofibroblasts (SEMFs) [13–16], endothelial cells [13, 17], vascular smooth muscle cells [13], and ill-defined inflammatory cells [18]. Despite this tremendous plasticity, the cellular origin of BMDCs, possible descendants from hematopoietic stem cell transplantation (HSCT), has not been referenced in any of the above studies. Some evidence implicates mesenchymal stem cells, also known as multipotent mesenchymal stromal cells (MSCs), in intestinal tissue repair following DSS or 2,4,6-trinitrobenzenesulfonic acid (TNBS) exposure. However, considerable uncertainty remains concerning the in vivo distribution and cell fate of donor-derived MSCs residing in either the recipient IECs [19] or SEMFs [20, 21], or in cells contributing to vasculogenesis such as endothelial cells [22]. Consequently, the tendency for repopulating cells to be scattered randomly in recipient intestinal tissues in different sources of HSCs and MSCs transplantation is curious.

Previously, using a DSS colitis with a myeloablation or busulphan (BU)-induced hypoplastic marrow model, we reported that susceptibility to DSS colitis was significantly increased by co-existing BU-induced bone marrow hypoplasia, an increase that was significantly reduced by enhancing epithelial engraftment of MSCs, an effect depending on restoring the epithelial barrier integrity rather than inhibiting host immune responses [19]. In other words, we have been unable to demonstrate any therapeutic effects of MSC against the inductive phase of acute DSS colitis without myeloablation, a finding in disagreement with previous reports [22–25]. Therefore, in this study, we focused on the role of transplanted MSCs in the repair stage of rat DSS colitis without myeloablation and determined both their in vivo distribution and fate in recipient colonic tissues and their therapeutic efficacy.

Methods

Experimental chemicals and animals

Jagged1 (R&D Systems, Inc., Minneapolis, MN), DAPT and SB431542 (Sigma-Aldrich Japan K.K., Tokyo Japan), and TGFβ-1 (PeproTech, Inc., NJ, USA) were purchased from the manufacturers. Lewis (Charles River Laboratories) and LEW-Tg [Gt (Rosa) 26Sor-lacZ] 44Jmsk rats [26], which express lacZ ubiquitously, were provided by the National BioResource Project for the Rat in Japan, Kyoto University (Kyoto, Japan), and were maintained according to the guidelines of the Committee for Animal Research of Sapporo Medical University. The Committee for Animal Research and for Security of Recombinant DNA Experiments of Sapporo Medical University reviewed and approved every experimental protocol. All rats were used when 7–8 weeks old and their weight was within 180–220 g.

Immunophenotype, in vitro differentiation, and fluorescent immunocytochemistry of rMSC

Rat MSCs (rMSCs) were harvested and cultured as described previously [27]. Briefly, bone marrow cells were harvested by inserting a needle into the shaft of the femurs and tibias, and flushing it with 30 ml of complete α-modified Eagle's medium (αMEM) containing 20% fetal bovine serum (FBS). Cell suspensions were filtered through a 70-μm nylon filter (Becton-Dickinson) and plated in 75-cm^2 flasks. Cells were grown in complete αMEM (20% FBS) at 37°C and 5% CO_2. After 3 days, the medium was replaced with fresh medium (10% FBS), and the adherent cells were grown to 80% confluency to obtain samples defined as passage 0. Cells between passage 3 and 5 were used for experiments. rMSCs immunophenotype was determined by FACSCalibur with antibodies specific for rat surface antigens, CD11b, CD31, CD43, CD44, CD45, and CD90 (Immunotech) [27]. The in vivo differentiation potential was confirmed as previously described [28] (data not shown). Immunofluorescent determination of α-smooth muscle actin (α-SMA, Thermo Scientific), desmin (Abcam), and vimentin (EPITOMICS) in MSCs was done using Texas Red®-labeled anti-IgG (H + L) antibody according to the manufacturer's instructions (data not shown).

Experimental colitis models and evaluation of severity of colitis

Dextran sulfate sodium colitis was induced by giving drinking water containing 4% DSS ad libitum for 7 days (day 0 to day 6). The DSS solution was replaced with water on day 6, and rats continued to drink regular water daily until they were evaluated by body weight, colon length, and histological scoring as follows: for inflammatory severity, none = 0; mild = 1; moderate = 2; and severe with inflammatory cell infiltrate was scored as 3. For inflammatory extent, the scores were none = 0, confined to mucosa = 1, mucosa and submucosa = 2, and transmural infiltrate = 3. For crypt damage, the scores were absence of damage = 0, basal 1/3 damaged = 1, and basal 2/3 damaged = 2; if the crypt was lost but surface epithelium was present, it was counted as 3, and a score of 3 was also given for both crypt and surface epithelium loss [9]. The pathologist [T.M.] blinded as to the grouping independently judged the histological score of most severely inflamed lesions for the colitis experiments and the corresponding anatomical segment of the colon for controls on representative sections stained with haematoxylin and eosin. Three whole-circumferential sections (total 90 sections) from each rat (n = 10) were fully examined.

RNA isolation and quantitative RT-PCR analysis

Total RNA was extracted using the RNeasy® Mini Kit (QIAGEN), and 1 μg total RNA was reverse-transcribed into cDNA with oligo-dT primers using the SuperScript® III Reverse Transcriptase (Invitrogen, Carlsbad, CA). Using Primer Express Software (Applied Biosystems, Foster City, CA), specific primers and probes were designed for rat *notch1, hes1, egf, tgfa, tgfb1, vegf, igf1, ptgs2, hgf, fgf2, tnfa, il1b, il10,* and *infg*, of which the rat-specific primers employed were deposited in the RTPrimerDB (http://medgen.ugent.be/rtprimerdb/) and are briefly described in supplementary Table 1 online. Rat *gapdh* primer, which acts as an internal standard for the integrity and the quantity of RNA, was purchased from Applied Biosystems (TaqMan GAPDH control reagent kit). Real-time PCR was performed in a GeneAmp 5700® Sequence Detection System SDS (Applied Biosystems) using SYBR® Green 1 PCR Master Mix (Applied Biosystems) for 40 cycles of a two-step PCR amplification (95°C for 15 s and 60°C for 1 min). Melting curves using Dissociation Curves software (Applied Biosystems) ensured only a single product was amplified. Data were analyzed using the amplification plot method, which involved calculation of the amplification efficacy by analyzing the change of fluorescence throughout the linear phase for every sample [29].

Western blot analysis of Notch signaling

Each segment of the rat colon was lysed in buffer that included 50 mmol/l Tris-HCl (pH 8.0), 150 mmol/l NaCl, and 0.5% NP40, 0.5% sodium deoxycholate, and Protease Inhibitor Cocktail Set III (Calbiochem). Forty micrograms of each lysate determined by a Bio-Rad protein assay (Bio-Rad) was resolved on a 12% denaturing polyacrylamide gel and transferred to a polyvinylidene difluoride (PVDF) membrane. After blocking with 5% nonfat dry milk in TBS, the membrane was incubated with primary antibodies against hes-1, then with horseradish peroxidase-conjugated secondary antibodies (Santa Cruz). Immunoreactivities were developed using the enhanced chemiluminescence kit (Amersham Biosciences).

LacZ-labeled rMSC transplantation

LacZ-labeled rMSCs were harvested from LEW-Tg [Gt (Rosa) 26Sor-lacZ] 44Jmsk rats as described above. Then 2×10^4 rMSCs/g in 500 μl αMEM was transplanted on the indicated day via a tail vein under anesthesia, while the control rats received 500 μl αMEM injection without rMSCs. MSC transplantation was principally performed once on day 2, except for one experiment exploring dose-dependency of MSC transplantation on therapeutic efficacy to body weight change; in this experiment MSCs were transplanted three times on day 2, 4, and 6 at the same above dosage, and one tenth dosage (2×10^3 rMSCs/g) was transplanted once on day 2.

Characterization of *lacZ*-labeled rMSCs in the recipient colonic tissue

The rats were killed by transcardial perfusion with 4% paraformaldehyde in PBS, and the colons were removed and fixed in the perfusion buffer for 24 h. After sucrose cryoprotection, OCT-embedded circumferential sections, 3 μm thick, were prepared for immunofluorescent determination of β-galactosidase (MP Biomedicals) using Texas Red®-labeled anti-IgG (H + L) antibody, CD31, CD45 (Santa Cruz), α-SMA (Thermo Scientific), desmin (Abcam), vimentin (EPITOMICS), RM-4 (TransGenic Inc) [30], and S-100 (COSMOBIO) using Alexa Fluor® 488-labeled secondary antibodies. Immunofluorescence was detected by LSM 510 META (Carl Zeiss), counterstained with DAPI (Vector Laboratories). Spectrum imaging analysis combined with confocal laser scanning microscopy was applied to lacZ-expressing cells or multicolor stained cells. Excitation wavelength was set at 561 nm for unstained sections and at 488/561 nm for immunofluorescence overlap-stained sections. To discriminate clearly lacZ-expressing or specific immunopositive cells from

autofluorescence, a fluorescence emission profile was obtained from each structure seen under confocal laser microscopy.

Analysis of cell cycle and apoptosis

Terminal deoxynucleotidyl transferase-mediated dUTP nick-end labeling (TUNEL) reactions were done using the DeadEnd Colorimetric TUNEL system (Promega). Proliferating cell nuclear antigen (PCNA) immunohistochemistry (Dako) was performed according to the manufacturer's instructions. The PCNA labeling index and apoptotic index were converted to percentages by counting PCNA-positive and TUNEL-positive nuclei of epithelial cells per five entire crypts in five different specimens, respectively, which corresponded to approximately 400–500 epithelial cells/specimen on average in this study.

Exposure of DSS to rMSC in culture

For in vitro differentiation induction, 0.5 or 1% dextran sulfate sodium (DSS, mol wt 40000) was added up to 3 weeks. For investigation on related signal transduction, MSCs were incubated in complete αMEM (10% FBS) with the addition of 2% DSS, Jagged1 (1 μm/ml), DAPT (50 μM) TGFβ-1 (0.1 ng/ml), and/or SB431542 (10 μM) at 37°C for 0, 24, and 72 h. MSCs were harvested at 0, 24, 72 h, and 3 weeks and analyzed by quantitative RT-PCR, immunofluorescence with confocal laser microscopy, or transmission electron microscopy.

Transmission electron microscopy

MSCs treated by 0.5% DSS for 3 weeks were centrifuged at 2000 g for 5 min and the pellet fixed with 2.5% glutaraldehyde/0.1 M PBS (pH 7.3) overnight at 4°C. After several rinses with PBS, the cells were postfixed in 1% osmium tetroxide at 4°C for 3 h and then rinsed thoroughly with distilled water, dehydrated by graded ethanol, and freeze-dried. The specimens were sputter-coated with platinum and observed with a transmission electron microscope (TEM, H-7500; Hitachi, Tokyo, Japan) operating at 10 kV.

Statistical analysis

To compare two groups, we performed parametric and nonparametric analyses using an unpaired *t* test and the Mann-Whitney *U* test, respectively. We compared categorical variables using the chi-square test, the exact *P* value based on Pearson's statistic, or the Monte Carlo method. In multiple comparisons, ANOVA followed by Bonferroni's test was applied. A difference was considered significant when $P < 0.05$ in all two-tailed tests. We used SPSS Statistics 17.0 (Chicago, IL, USA) for all statistical tests.

Results

After confirming the immunophenotype of $CD90^+$ and that the differential capacity of rMSC isolates was consistent with those of previous reports (data not shown) [27], we investigated the therapeutic efficacy of rMSCs transplants in rats with 4%-DSS acute colitis, including the recovery phase (Fig. 1). There was no effect on the inductive phase of acute colitis during exposure to DSS (day 0 to day 6), but during recovery when DSS was discontinued, body weight restoration was modestly but significantly promoted by rMSC transplantation (Fig. 1a). A dose-dependent therapeutic effect of rMSC transplantation on body weight change is clearly shown in Fig. 1b. Since statistically significant differences developed on day 9 or later, we chose day 9 for histologic assessment. Epithelial injury was markedly reduced in the rMSC transplanted rats (Fig. 2a–c), whose total histological score was significantly decreased compared to those not transplanted (Fig. 2d). rMSC transplantation significantly increased PCNA-positive cells (Fig. 2e–h) and markedly decreased TUNEL-positive cells (Fig. 2i–l).

Next, we explored the mechanisms for the therapeutic action of transplanted rMSCs by comparing growth factor and cytokine profiles in rats in the recovery phase of 4% DSS colitis with and without rMSC transplantation (Fig. 3a). In the whole colonic tissues analyzed by quantitative RT-PCR, there were no significant differences between treated and untreated rats except for *tgfa*, which was significantly increased by rMSC transplantation. Alcian blue staining revealed that goblet cells were decreased in colonic tissues without MSC transplantation, but were excessively recovered with transplantation, although colonic epithelial cell hyperplasia and crypt elongation were still observed (Fig. 3b–d). Notch signaling (*notch1* and *hes1*) was significantly inhibited by MSC transplantation (Fig. 3e–g).

On day 9, 3 days after DSS cessation, β-galactosidase-expressing cells were infrequently detected in the stroma of laminar propria mucosa (Fig. 4). The scarce rMSC-derived cells were identified by the emission fingerprinting method in comparison with the reference spectra of Texas Red®-labeled rMSC as depicted in Fig. 4c, m, n in detail. Immunofluorescence double staining with Texas Red®-labeled β-galactosidase antibody and Alexa Fluor® 488-labeled antibodies against α-SMA (Fig. 4a–d), desmin (Fig. 4e–h), vimentin (Fig. 4i–l), CD31 (Fig. 5a–d), CD45 (Fig. 5e–h), RM-4 (Fig. 5i–l), and S-100 (data not shown) disclosed that the stromal β-galactosidase-positive cells were αSMA^+, $desmin^+$, and $vimentin^+$, as shown in Fig. 4,

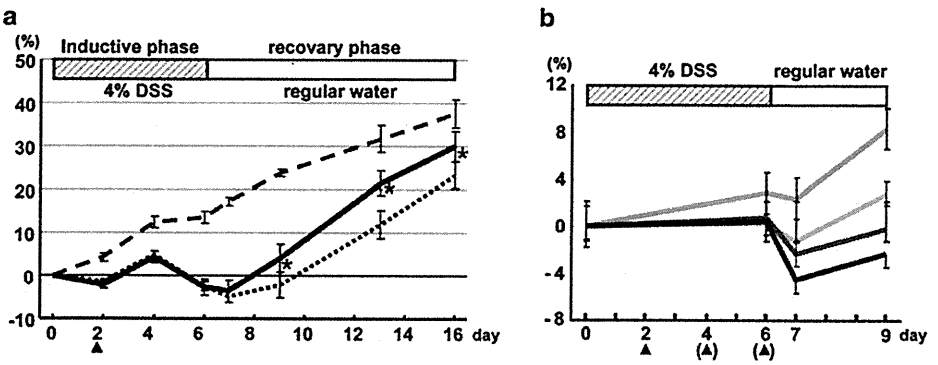

Fig. 1 Therapeutic effect of rMSC transplantation in the recovery phase of acute DSS colitis. **a** Time course of body weight change and therapeutic protocol in the recovery phase of acute DSS colitis. *Closed arrowheads* on day 2 represent rMSCs transplantation. The rats were killed on day 9 for histological analysis. *Asterisks* represent statistical significance between rats with MSC transplantation (MSC+) and without MSC transplantation (MSC− groups) ($P = 0.003$ at day 9, $P = 0.0006$ at day 13 and $P = 0.001$ at day 16). *Broken*, *solid*, and *dotted lines* represent body weight of normal (untreated), MSC+, and MSC− groups ($n = 10$, each for **a**). *Error bar* represents mean ± SE. **b** Dose-dependent therapeutic effect on body weight change. The *red line* indicates body weight change of the rats transplanted three times at day 2, 4, and 6 at the indicated dose. The *orange line* represents the rats with regular transplantation on day 2. The *green line* indicates the rats transplanted with one tenth dose on day 2. The *black line* represents control rats without transplantation. All groups comprise three rats

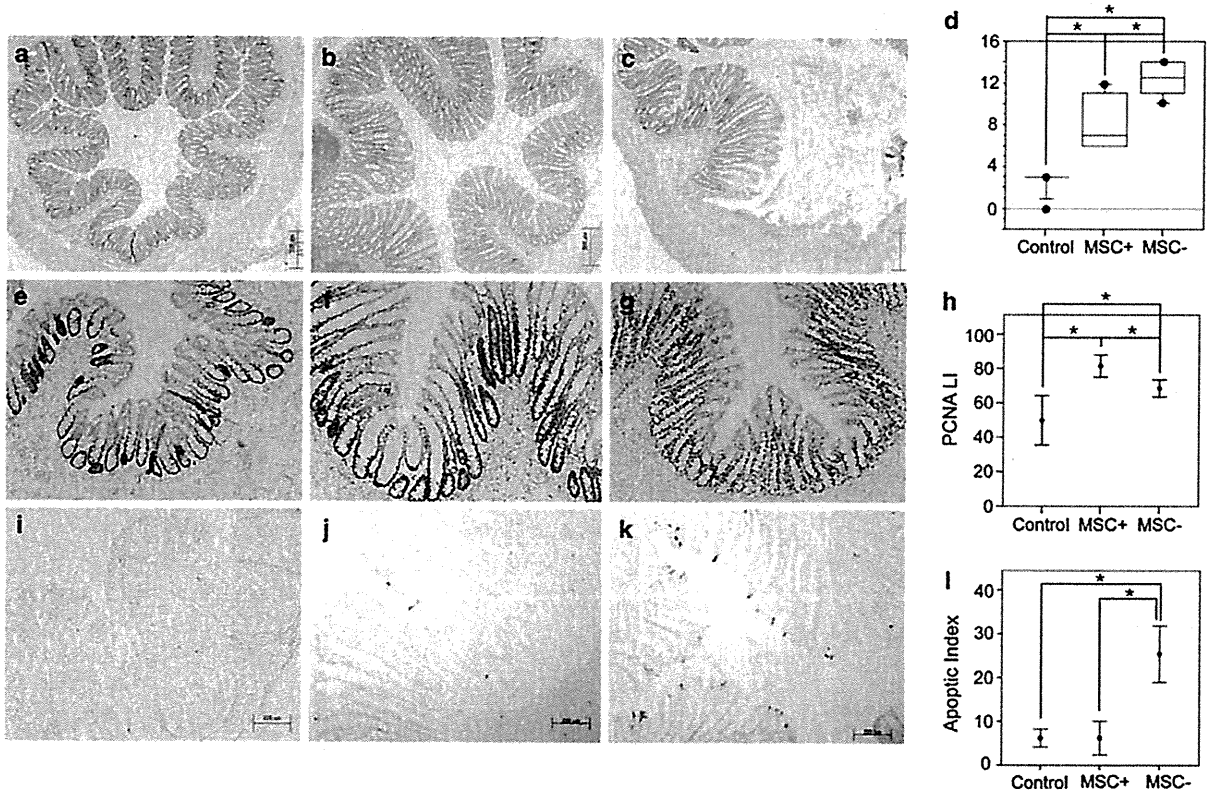

Fig. 2 Histological and cell cycle analysis on rMSCs transplantation. **a–c** Comparison of representative histopathology on rMSC transplantation. **d** Histological scores in control (2.6 ± 1.1), MSC+ (8.2 ± 2.6), and MSC− (12.3 ± 1.9) groups. *Asterisks* represent statistical significance (control vs. MSC+: $P = 1.27E\text{-}4$, control vs. MSC−: $P = 8.87E\text{-}8$, MSC+ vs. MSC−: $P = 0.004$). **e–g** Immunofluorescence analyses against PCNA. **h** PCNA labeling index. *Asterisks* represent statistical significance (control vs. MSC+: $P = 6.21E\text{-}7$, control vs. MSC−: $P = 1.31E\text{-}4$, MSC+ vs. MSC−: $P = 0.003$). **i–k** Photomicrographs of representative sections of TUNEL analysis. **l** apoptotic index. *Asterisks* represent statistical significance (control vs. MSC−: $P = 6.84E\text{-}6$, MSC+ vs. MSC−: $P = 6.86E\text{-}6$). **a**, **e**, **i** were from the control, **b**, **f**, **j** were from a rat transplanted with rMSC (MSC+), and **c**, **g**, **k** were from the rat without transplantation (MSC−)

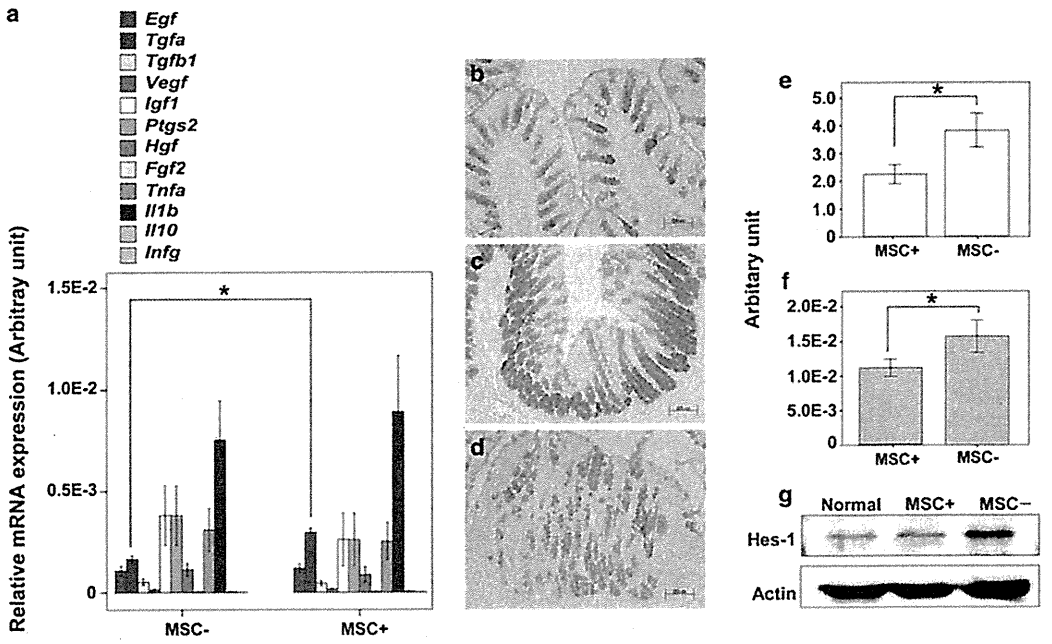

Fig. 3 Comparative analyses of cytokines, growth factors, and Notch signaling pathway. Comparative analysis of cytokines and growth factors on whole colonic tissues from MSC+ and those from MSC− groups (**a**). *Asterisks* on *tgfa* represent statistical significance between MSC+ and MSC− groups ($P = 0.003$). Alcian blue staining of the representative sections from normal rats (**b**), MSC transplanted rat (MSC+) (**c**), and sham transplanted rat (MSC−) (**d**). Quantitative RT-PCR analysis of *notch1* (**e**) and *hes1* (**f**). *Asterisks* represent statistical significance between rats MSC+ and MSC− groups ($P = 0.03$ and $P = 0.04$ in **e** and **f**, respectively). Western blot analysis of hes-1 (**g**)

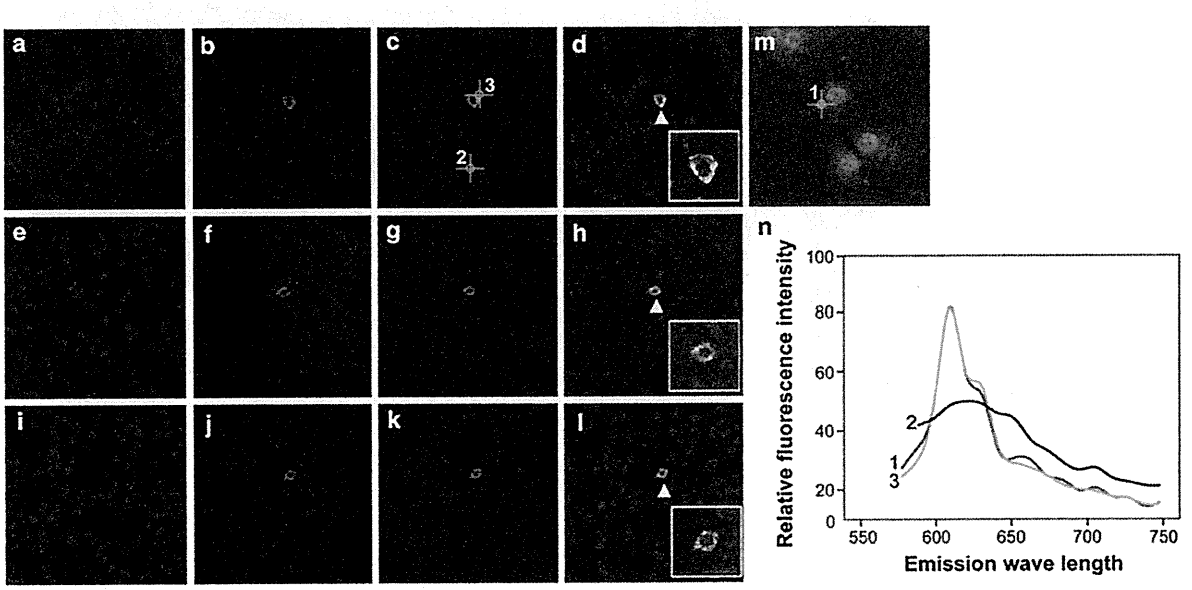

Fig. 4 Characterization of donor-derived rMSCs in recipient colonic tissue fluorescent immunocytochemistry of rMSCs using emission wave length fingerprinting. Immunofluorescence double staining with Texas Red®-labeled β-galactosidase antibody (**c**, **g**, **k**) and Alexa Fluor® 488-labeled α-SMA (**b**), desmin (**f**), and vimentin (**j**) antibody. **a**, **e**, **i** Show counter nuclear staining with DAPI (×600). *White arrowheads* in a merged image of **d**, **h**, **l** indicate double staining positive, yellow fluorescent cells in the stroma shown in a higher magnification view of the area enclosed by a *rectangle*, respectively. **m** Fluorescent immunocytochemistry of rMSC where emission wave length fingerprinting was performed at the marked position as the positive reference of Texas Red® signal (digit 1). Representative colonic section (**c**) of rMSC transplantation where two marked positions were examined, and the result is depicted in **n**, one for background reference signal (digit 2) and the other (digit 3) for the experimental object

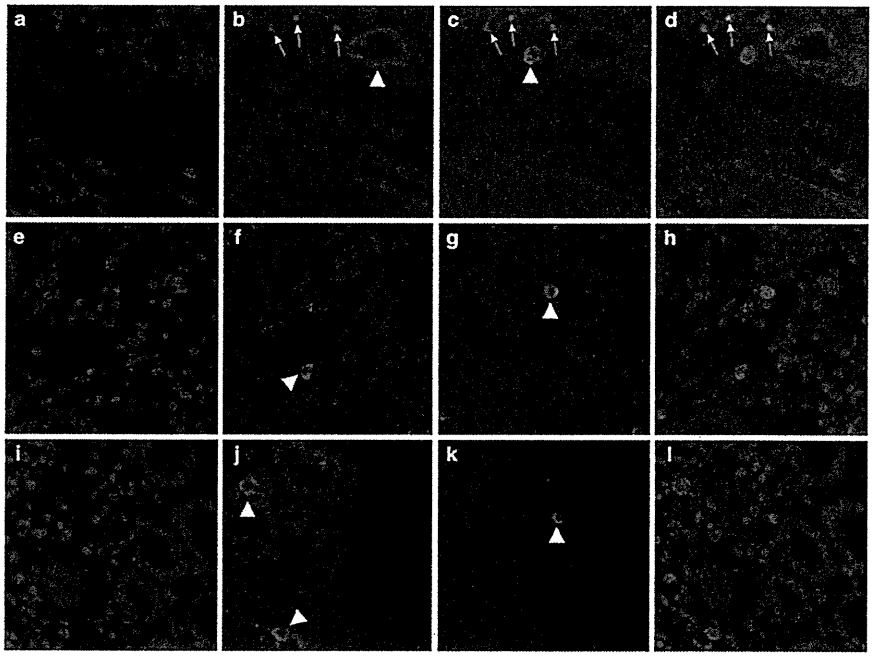

Fig. 5 Characterization of donor-derived rMSCs in recipient colonic tissues. Immunofluorescence double staining with Texas Red®-labeled β-galactosidase antibody (**c**, **g**, **k**) and Alexa Fluor® 488-labeled CD31 (**b**), CD45 (**f**), and RM-4 (**j**) antibody. **a**, **e**, **i** Show counter nuclear staining with DAPI (×600). *White arrowheads* in **b**, **c**, **f**, **g**, **j**, **k** indicate positive fluorescence staining signals by the above antibodies. *White arrows* in **b**, **c** indicate non-specific false-positive signals emitted by granulocytes

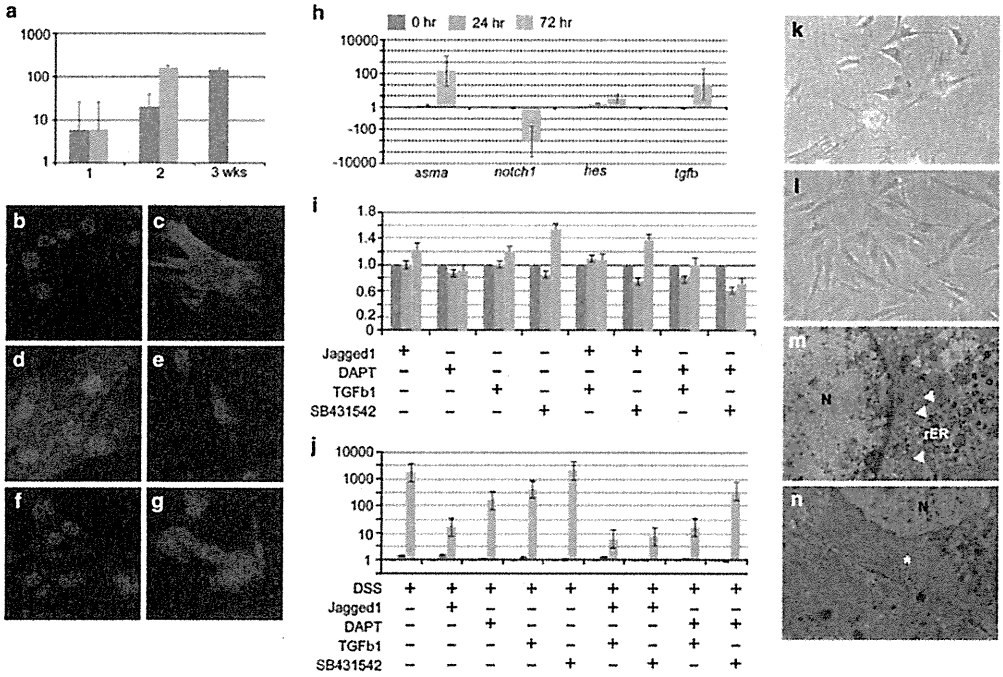

Fig. 6 Induction of αSMA in MSC in vitro. For in vitro α-SMA induction, 0.5% (*blue bar*) or 1% DSS (*pink bar*) was added to media up to 3 weeks, and results from real-time RT-PCR of *αsma* transcripts were depicted in a semi-logarithmic (the arbitrary unit) graph in **a**. α-SMA (**b**, **c**), desmin (**d**, **e**), and vimentin (**f**, **g**) of Texas Red®-based fluorescent immunocytochemistry for untreated (**b**, **d**, **f**) and exposed by 2% DSS for 72 h on rMSCs (**c**, **e**, **g**). *αSMA* transcript was potently induced by exposure of 2% DSS for 72 h, along with decreased *notch1*, and increased *tgfb* and *hes1* transcripts (**h**). Effects of notch1 and *tgfb* signaling on α-SMA in rMSC were examined in vitro with DSS (**j**) and without DSS (**i**). Morphological changes caused by 2% DSS for 72 h exposure were observed by phase-contrast microscopy (**l**) and TEM (**n**) in comparison to untreated MSC (**k**, **m**), respectively. *Orange* and *white arrowheads* indicate mitochondria (*Mit*) and rough endoplasmic reticulum (*rER*), respectively

while the other markers examined were negative, as shown in Fig. 5, and were identified as myogenic lineage cells, such as smooth muscle-, pericyte-, or myofibroblast-like cells.

As depicted in Fig. 6a, exposure of 0.5% DSS time-dependently induced αSMA expression for 3 weeks, while 1% DSS exposure was too toxic for rMSCs to survive, so that *αsma* transcript became undetectable at 3 weeks. Exposure of cells to 2% DSS for 72 h rapidly and maximally induced *αsma* transcript in our setting (data not shown), and induced the expression of αSMA, desmin, and vimentin (Fig. 6b–g) along with potently decreasing *notch1* transcript, whereas the *tgfb1* transcript was strongly and *hes1* weakly upregulated (Fig. 6h). Based on these findings, we asked whether the induction of αSMA in rMSCs depended on Notch and/or TGFβ signaling (Fig. 6i, j), and finally determined the cell fate of rMSC in vitro (Fig. 6k–n). DSS proved to be the most potent inducer of αSMA in rMSCs among the factors examined and induced spindle-shape morphology (Fig. 6l) and abundant myofilaments (Fig. 6n) with focal densities in their cytoplasms.

In contrast to these results, no significant therapeutic benefits were observed in the acute phase of either 10% DSS lethal colitis or 4% DSS colitis rats transplanted with rMSC (Supplementary Fig. 1 online).

Discussion

Ample evidence suggests BMDCs contribute to intestinal repair processes in both humans [11, 12, 14] and animals [14], while the role of MSCs in recipient colonic tissues remains uncertain. Contrary to our original expectations and recent studies, in which we have observed a favorable outcome of MSC therapy against DSS colitis [22–25], we consistently failed to show any significant therapeutic effect of MSCs against the inductive phase of acute DSS colitis (Fig. 1a, Supplementary Fig. 1 online) [19]. In contrast, we report a novel observation of a modest but significant dose-dependent promotion of repair from 4% DSS colitis by MSC transplantation. Furthermore, we observed an increase in *tgfa* transcript with suppression in Notch signaling in colonic tissue taken from DSS animals with MSC transplantation. In this study, rMSCs which are only occasionally engrafted into the stroma of the laminar propria mucosa, are likely reprogrammed to differentiate into myogenic lineage cells, such as pericytes, vascular smooth-muscle cells, or myofibroblasts [31].

Although DSS colitis repair was accentuated by successful engraftment of rMSCs, among the expression profiles of the relevant growth factor and cytokine transcripts examined, only *tgfa* transcripts increased significantly in the whole colonic tissues (Fig. 3a). TGFα, a member of the EGF superfamily, has structural and functional homology to EGF and activates the EGF receptor (EGFR) [32]. TGFα is expressed in multiple cell types, such as epithelial cells and macrophages, which act directly on the IECs to stimulate proliferation and migration. How can these findings be explained given the paucity of TGFαs derived from the few engrafted rMSCs? Perhaps TGFα upregulation in cell types other than rMSCs, possibly IECs, in response to inflammation is sufficient explanation, with subsequent release into the site of injury where it may contribute to wound healing or intestinal adaptation [33].

Goblet cell depletion caused by impaired secretory cell differentiation during acute DSS colitis was prevented via inhibition of Notch by MSC therapy even as early as 3 days after DSS cessation, when colonic epithelial cell hyperplasia and crypt elongation were still present, reflecting an intense driving force of epithelial cell proliferation. The activation of Notch promoted proliferation of crypt progenitor cells and directed their cell fates toward absorptive but not secretory lineage cells [34]. This was consistent with a previous finding that Notch signaling was activated in a greater number of IECs in DSS colitis, which might be closely related with the greater number of proliferating IECs and the loss of mucin-producing IECs [35]. Our finding that Notch signaling of inflamed crypts including intestinal stem and progenitor cells was partially suppressed by MSC therapy, which directed recovery of secretory progenitors and ultimately mature goblet cells, along with maintaining IEC proliferation [8]. Mechanisms modulating the Notch signaling pathway in response to MSCs warrant further investigation.

Unfortunately, the current study fails to resolve the critical paradox that a substantial beneficial effect on the repair of colitis was observed despite the disproportionally low transplantation efficiency of MSCs. Considering how rare repopulating MSCs could effectively enhance the global regenerative responses, such as promoted proliferation, suppressed apoptosis, and corrected secretary cell differentiation in damaged crypts, leads us to the appealing speculation that MSCs would complement and help promote functions exerted by endogenous intestinal stem cells as niche cells. In contrast with previous reports including our own, we furthermore found that transplanted rMSCs were seldom engrafted into epithelial cells [11, 12, 19], SEMFs [14], or cells contributing to vasculogenesis, such as endothelial cells [22]. Although there are many recent reports of the beneficial effects of BMDCs on experimental colitis in various settings, including murine DSS [22–24] and 2,4,6-trinitrobenzene sulfonic acid (TNBS) colitis [36], rat DSS [25] and TNBS colitis [20, 37], and rat DSS colitis with bone marrow hypoplasia [19], distribution or cell fate of donor-derived cells varies extremely depending upon each individual study. These partially reflect differences in species, transplantation procedures, conditioning protocols,

and finally detection methods. However, considering possible therapeutic applications of MSC therapy for clinical intestinal disorders, these enigmas must be solved.

In this study, in vivo rMSCs expressed the following three stromal markers in their cytoplasm: α-SMA, desmin, and vimentin (Fig. 3). Since immunofluorescence of rMSCs was originally positive for desmin, weakly positive for vimentin, and negative for α-SMA in nonstimulated culture at least up to passage 5 (Fig. 6a, c, e), it is likely they were reprogrammed to myogenic lineage differentiation triggered by signals from the micro-milieu in the recipient inflamed tissues. Considering the ability of vascular accessory cells or myofibroblasts to enhance tissue healing, it was suggested that myogenic differentiated rMSCs were likely to be involved in intestinal repair. Furthermore, follow-up for at least a year after rats received MSC transplants suggests a negligible risk of induced colon cancer. It raises the possibility that MSCs would be therapeutically applicable in IBD.

In vitro exposure of rMSCs to DSS dramatically upregulated α-SMA in a time-dependent and possibly dose-dependent manner (Fig. 6a, h), suppressed Notch signaling, and simultaneously enhanced *tgfb1* expression (Fig. 6h) while changing the cells structure from abundant cytoplasms with prominent processes (Fig. 6k) to thin spindle-shaped morphology (Fig. 6l). Notch signaling normally maintains mesenchymal progenitors while suppressing osteoblast differentiation in bone marrow [38], and TGF-β1 stimulates expression of α-SMA, which is a marker gene for smooth muscle cells or myofibroblasts, in bone marrow-derived MSCs in vitro [39]. Consequently, upregulation of *tgfb* with simultaneous inhibition of the Notch signaling pathway by DSS exposure is likely to favor rMSCs differentiation into myogenic lineage cells. Although DSS proved to be the most potent inducer of α-SMA beyond the physiological regulation of Notch and TGF-β signaling (Fig. 6i, j), unfortunately, 3-week-long exposure to 0.5% DSS was not an optimal choice to determine whether rMSCs finally differentiated into smooth muscle cells, pericytes, or myofibroblasts on transmission electron microscopy (Fig. 6m, n).

In conclusion, MSCs can be active and beneficial cellular participants in intestinal organ repair by direct stromal cell differentiation. Further characterization of MSC-derived myogenic cells in DSS colitis is warranted with the goal of cell-based therapy as a new approach to the treatment of IBD.

Acknowledgments We are very grateful to Dr. T Mitsuhashi, associate professor of the Department of Surgical Pathology, for assessment of colitis and Dr. M Murata, assistant professor of the Second Department of Pathology, Sapporo Medical University, for performing the electron microscopy studies. We are thankful to the National BioResource Project for the Rat in Japan (http://www.anim.med.kyoto-u.ac.jp/NBR/) for providing rat strains LEW-Tg (Gt (Rosa) 26Sor-lacZ) 44Jmsk. This work was supported in part by Health and Labor Sciences Research Grants for research on intractable diseases from Ministry of Health, Labor and Welfare of Japan (K.I.).

Conflict of interest None of the authors has any conflicts of interest.

References

1. Okayasu I, Hatakeyama S, Yamada M, Ohkusa T, Inagaki Y, Nakaya R. A novel method in the induction of reliable experimental acute and chronic ulcerative colitis in mice. Gastroenterology. 1990;98:694–702.
2. Watt J, Marcus R. Experimental ulcerative disease of the colon. Methods Achiev Exp Pathol. 1975;7:56–71.
3. Egger B, Bajaj-Elliott M, MacDonald TT, Inglin R, Eysselein VE, Buchler MW. Characterization of acute murine dextran sodium sulphate colitis: cytokine profile and dose dependency. Digestion. 2000;62:240–8.
4. Cooper HS, Murthy SNS, Shah RS, Sedergran DJ. Clinicopathologic study of dextran sulfate sodium experimental murine colitis. Lab Invest. 1993;69:238–49.
5. Sturm A, Dignass AU. Epithelial restitution and wound healing in inflammatory bowel disease. World J Gastroenterol. 2008;14:348–53.
6. Taupin D, Podolsky DK. Trefoil factors: initiators of mucosal healing. Nat Rev Mol Cell Biol. 2003;4:721–32.
7. Dignass AU, Tsunekawa S, Podolsky DK. Fibroblast growth factors modulate intestinal epithelial cell growth and migration. Gastroenterology. 1994;106:1254–62.
8. Scoville DH, Sato T, He XC, Li L. Current view: intestinal stem cells and signaling. Gastroenterology. 2008;134:849–64.
9. Williams KL, Fuller CR, Dieleman LA, DaCosta CM, Haldeman KM, Sartor RB, et al. Enhanced survival and mucosal repair after dextran sodium sulfate-induced colitis in transgenic mice that overexpress growth hormone. Gastroenterology. 2001;120:925–37.
10. Komori M, Tsuji S, Tsujii M, Murata H, Iijima H, Yasumaru M, et al. Involvement of bone marrow-derived cells in healing of experimental colitis in rats. Wound Rep Reg. 2005;13:109–18.
11. Okamoto R, Yajima T, Yamazaki M, Kanai T, Mukai M, Okamoto S, et al. Damaged epithelia regenerated by bone marrow-derived cells in the human gastrointestinal tract. Nat Med. 2002;8:1011–7.
12. Matsumoto T, Okamoto R, Yajima T, Mori T, Okamoto S, Ikeda Y, et al. Increase of bone marrow-derived secretory lineage epithelial cells during regeneration in the human intestine. Gastroenterology. 2005;128:1851–67.
13. Brittan M, Chance V, Elia G, Poulsom R, Alison MR, MacDonald TT, et al. A regenerative role for bone marrow following experimental colitis: contribution to neovasculogenesis and myofibroblasts. Gastroenterology. 2005;128:1984–95.
14. Brittan M, Hunt T, Jeffery R, Poulsom R, Forbes SJ, Hodivala-Dilke K, et al. Bone marrow derivation of pericryptal myofibroblasts in the mouse and human small intestine and colon. Gut. 2002;50:752–7.
15. Bamba S, Lee C-Y, Brittan M, Preston SL, Direkze NC, Poulsom R, et al. Bone marrow transplantation ameliorates pathology in interleukin-10 knockout colitic mice. J Pathol. 2006;209:265–73.